ESCRT-III controls nuclear envelope reformation

Yolanda Olmos[1], Lorna Hodgson[2], Judith Mantell[2,3], Paul Verkade[2,3,4] and Jeremy G Carlton[1]*

1. Division of Cancer Studies,
Section of Cell Biology and Imaging
King's College London
London
SE1 1UL

2. School of Biochemistry
University of Bristol
Medical Sciences Building
University Walk
Bristol
BS8 1TD

3. Wolfson Bioimaging Facility
University of Bristol
Medical Sciences Building
University Walk
Bristol
BS8 1TD

4. School of Physiology & Pharmacology
University of Bristol
Medical Sciences Building
University Walk
Bristol
BS8 1TD

*Correspondence : Jeremy.Carlton@kcl.ac.uk

Running Title : ESCRTs and the nuclear envelope

Key Words : Cell Biology, Mitosis, ESCRT, Nuclear Envelope, Cell Division

Abstract

During telophase, the nuclear envelope (NE) reforms around daughter nuclei to ensure proper segregation of nuclear and cytoplasmic contents[1-4]. NE reformation requires the coating of chromatin by membrane derived from the Endoplasmic Reticulum and a subsequent annular fusion step to ensure the formed envelope is sealed[1,2,4,5]. How annular fusion is accomplished is unknown, but it is thought to involve the p97 AAA-ATPase complex and bears a topological equivalence to the membrane fusion event that occurs during the abscission phase of cytokinesis[1,6]. We find here that the Endosomal Sorting Complex Required for Transport-III (ESCRT-III) machinery localises to sites of annular fusion in the forming NE and is necessary for proper post-mitotic nucleo-cytoplasmic compartmentalisation. The ESCRT-III component Charged Multivesicular Body Protein (CHMP) 2A is directed to the forming NE through binding to CHMP4B and provides an activity essential for NE reformation. Localisation also requires the p97 complex member Ubiquitin Fusion and Degradation 1 (UFD1). Our results describe a novel role for the ESCRT-machinery in cell division and demonstrate a conservation of the machineries involved in topologically equivalent mitotic membrane remodeling events.

Main Text

The ESCRT-III complex performs a topologically unique membrane fusion, allowing release of enveloped retroviruses during viral budding, intraluminal vesicles during multivesicular body biogenesis, and daughter cells during the abscission phase of cytokinesis[7-11]. We found that as well as localising to the midbody during late cytokinesis, endogenous ESCRT-III components CHMP2A and CHMP2B encircled the forming daughter nuclei during telophase (Figure 1A, 1B and Extended Data Figure 1A). CHMP2A localisation was sensitive to CHMP2A-targeting siRNA (Extended Data Figure 1B) and was not continuous; rather we found that CHMP2A adopted a transient punctate localisation around the decondensing nuclei during telophase (Extended Data Figure 1C, Supplementary Video 1). By scoring localisation in HeLa cells stably expressing mCh-tubulin, (cell cycle of 21.5 ± 1.7 hours, n = 93), we estimate the duration of CHMP2A localisation to be 96 ± 8.9 seconds. We found cells expressing GFP-CHMP4B[12] also displayed a transient, punctate, juxta-nuclear localisation during telophase with recruitment of GFP-CHMP4B lasting 225 ± 66 seconds (n = 8, ± S.D.) and individual puncta lasting 75 ± 46 seconds (n = 92, ± S.D., Extended Data Figure 1D, Supplementary Video 2). Telophase ESCRT-III localisation was observed in other cell lines, including human-diploid fibroblasts (Extended Data Figure 1E). Using HeLa cells stably expressing a Yellow Fluorescence Protein (YFP)-tagged nuclear envelope marker (Lamin Associated Protein 2β, YFP-LAP2β)[13], we determined that the juxtanuclear localisation corresponded to the forming nuclear envelope. Here, we observed colocalisation with the Lamin B Receptor (LBR)[14] (Figure 1C) and demonstrated that CHMP2A localisation occurred prior to appreciable formation of a nuclear lamina or nuclear pore complexes (Extended Data Figure 1F and 1G). Whilst mitotic chromatin association of ESCRT-III has been previously

reported[15], its function remains unknown. To investigate the role of ESCRT-components at the NE, we employed siRNA to deplete these proteins[16]. As described previously[17], depletion of ESCRT-components produced aberrant nuclei and these defects phenocopied those produced by depletion of proteins required for NE reformation (Extended Data Figure 1H)[18]. NE-reformation is thought to be a two-phase process, separable into membrane fusion events that create an expanding reticular network with subsequent annular fusion of holes within this network to create a sealed barrier[1]. We next employed correlative light-electron microscopy (Extended Data Figure 2A-D) to examine telophase ESCRT-III NE-localisation. We found that at the stage of ESCRT-III recruitment, the NE had incompletely formed (Figure 1D). Two populations of CHMP2A-positive membranes were found. Firstly, isolated CHMP2A-decorated vesicles were observed in the cytoplasm, proximal to the forming NE (5.7 ± 4.2 % of total cellular gold, Extended Data Figure 2Ei). Secondly, CHMP2A-decorated double-membrane sheets were observed to coat the chromatin (51 ± 1.7 % of total cellular gold was within 100 nm of the NE). On these sheets, CHMP2A localised to discrete regions, with intact NE being devoid of label, but with CHMP2A preferentially (Extended Data Figure 2H) decorating nucleo-cytoplasmic channels (mean diameter 38.4 ± 12.5 nm (n = 2 ± S.E.M., from 17 determinations)) between the forming double membranes of the NE (Figure 1D, Extended Data Figure 2D-2G, Extended Data Figure 3A-D, Supplementary Videos 3 and 4). These channels must be resolved through annular fusion and given the observed localisation and topological equivalence with cytokinetic abscission (Figure 1E), we speculated that ESCRT-III might be involved in this process.

Requirements for CHMP2A localisation to the telophase NE were revealed through depletion of partner ESCRT-proteins, with CHMP4B and CHMP3, as for other ESCRT-dependent membrane remodeling events, playing a major role in this recruitment (Figure 2A). We employed siRNA-resistant FLAG-tagged CHMP2A expressed at near-endogenous levels to report localisation in the presence of CHMP2A siRNA (Figure 2B and 2C). Through introduction of mutations targeting known binding-partners, we found, as for midbody recruitment and cytokinetic abscission (Extended Data Figure 4A and 4B), and consistent with the previously determined telophase localisation of GFP-CHMP4B (Extended Data Figure 1D), that whilst $CHMP2A^{R}$-FLAG localised to the forming NE, disrupting interaction with CHMP4 proteins by mutation of Arg24, Arg27 and Arg31 to Ala ($CHMP2A^{R}$-FLAG RRR-AAA)[16] abolished this localisation. Mutation of the N-terminal CHMP2A α_0 helix[19], or residues involved in the interaction with VPS4[16] had no effect on NE localisation (Figure 2C, Extended Data Figure 4A). These data indicate that CHMP2A is recruited to the forming NE through classical assembly of the ESCRT-III complex.

The p97 AAA-ATPase controls both phases of NE reformation; in concert with its adaptor protein p47, it regulates membrane delivery and NE expansion whilst through its adaptors Nuclear Protein Like 4 (NPL4) and UFD1 it regulates annular fusion[6]. Through NPL4 and UFD1, the p97 complex extracts ubiquitinated Aurora-B, a Chromosomal Passenger Complex (CPC) component, from chromatin to allow chromatin

decondensation and membranation[20,21]. Given our observed ESCRT-III localisation (Figure 1) and known interactions of ESCRT-III components with the CPC[13], we screened the ESCRT-machinery for interaction with the p97 complex by yeast 2-hybrid assay (Extended Data Figure 5A-D). We found that CHMP2A bound specifically to UFD1 and confirmed this interaction by direct-binding and co-precipitation assays (Figure 3A, 3B and Extended Data Figure 5E-H). We mapped the interaction with CHMP2A to the C-terminus of UFD1 (Extended Data Figure 5F and 5G) and found that truncation of the C-terminus of CHMP2A, or removal of the autoinhibitory helix (α5), prevented interaction with UFD1 (Figure 3A). We employed siRNA targeting UFD1 (Extended Data Figure 6A); although its partner protein, p97, was required for EGFR degradation[22], we found cells depleted for UFD1 degraded EGFR normally (Extended Data Figure 6B), allowed release of HIV-1 based lentivirus (Extended Data Figure 6C), and as previously reported[21], completed cytokinesis normally (Extended Data Figure 6D). However, whilst cells depleted for UFD1 recruited CHMP2A to the midbody (Figure 3D), recruitment of CHMP2A to the forming NE was impaired (Figure 3C and 3D).

To examine mitotic roles for ESCRT-III in NE reformation, we imaged synchronised cultures of cells stably expressing Histone 2B-mCherry (H2B-mCh) and YFP-LAP2β and quantified the time taken to enclose the chromatin with YFP-LAP2β positive nuclear envelope. We were surprised to find that cells lacking ESCRT-III, but not UFD1, enclosed their chromatin faster than control cells (Extended Data Figure 7A-C). To explore the integrity of the nascent NE in CHMP2A depleted cells, we followed a protocol similar to that recently described[23] and imaged synchronised cultures of HeLa cells stably expressing both H2B-mCh and GFP-tagged β-Galactosidase (β-Gal) fused to the nuclear localisation signal (NLS) from Simian Virus 40 (GFP-NLS-βGal)[24]. GFP-NLS-βGal is released from the nucleus upon NE breakdown at mitotic onset and returned upon formation of transport-competent nuclear pores during NE reformation (Extended Data Figure 8A and 8B). We found that the rate of GFP-NLS-βGal return to the nucleus was slower in ESCRT-III-depleted cells (Figure 4A-C), despite the cells having enclosed their chromatin with NE membranes faster (Extended Data Figure 7A). Whilst nuclei were frequently malformed in ESCRT-III-depleted cells (Extended Data Figure 1H[17]), incorporation of nuclear pore complexes and import machineries were normal (Extended Data Figure 8C-8E). However, in CHMP2A-, CHMP3- or UFD1-depleted cells, the post-mitotic nucleo-cytoplasmic partitioning of GFP-NLS-βGal was reduced (Figure 4B and 4C, Extended Data Figure 9A and 9B), indicating that NE integrity was compromised by treatments that prevent ESCRT-III assembly at the NE. Results were confirmed with a second reporter (GFP-NLS) (Extended Data Figure 9C) and we demonstrated that nuclear retention of this probe was defective in post-mitotic ESCRT-III depleted cells (Extended Data Figure 9D and 9E). Using correlative live-cell electron tomography, we found that CHMP2A depletion resulted in the persistence of unsealed holes in the post-mitotic NE (Figure 4D and 4E and Extended Data Figure 10A and 10B). Paralleling CHMP2 requirements in lentiviral release and cytokinetic abscission (Extended Data Figure 6C, and Extended Data Figure 9F), depletion of CHMP2B had

minimal effect upon NE integrity (Extended Data Figure 9A and 9B), whilst co-depletion of CHMP2A and CHMP2B disrupted NE integrity to a greater extent than CHMP2A depletion alone (Figure 4B). NE integrity could be rescued by stable expression of siRNA-resistant CHMP2A-FLAG (CHMP2A^{R}-FLAG), but, as with CHMP2A requirements in cytokinesis (Extended Data Figure 4B) and HIV-1 release[16], not by expression of CHMP2A^{R}-FLAG RRR-AAA (Figure 4F and 4G). We describe a novel localisation and function of ESCRT-III in NE remodeling at sites of annular fusion, a process strikingly similar to classical ESCRT-III mediated membrane remodeling (Extended Data Figure 10C). Localisation is governed by classical ESCRT-III assembly mechanisms and also requires UFD1. An equivalent ESCRT-III-dependent membrane remodeling at the NE may allow viruses or megaRNPs to traverse this membrane[25-27] and in yeast, ESCRT-III has recently been shown to participate in surveillance and extraction of defective nucleoporins at the IMN[28] indicating additional ESCRT-III activities on this membrane may exist throughout the cell cycle. ESCRT-III is thus involved in regulating the quality of the NE and gene expansion within the ESCRT-machinery may have resulted from an evolutionary drive to accommodate open mitoses.

Acknowledgements

JCG is a Wellcome Trust Research Career Development Fellow. We acknowledge the Nikon Imaging Centre at KCL and the NIHR Comprehensive Biomedical Research Centre at Guy's and St Thomas' NHS Foundation Trust for access to core equipment. We thank the staff of the Wolfson Bioimaging Facility for their support. We thank Prof Juan Martin-Serrano (KCL) for gifts of plasmids and cells.

Author Contributions

JGC conceived the study. PV, LH and JM designed, performed and analysed electron microscopy experiments. JGC and YO designed, performed and analysed data from other experiments. JGC wrote the manuscript with assistance from all other authors.

Figure Legends

Figure 1 : ESCRT-III localises to the forming nuclear envelope

A. HeLa cells stained with anti-tubulin, either anti-CHMP2A or anti-CHMP2B and 4',6-diamidino-2-phenylindole (DAPI). Scale bar is 10 μm, images representative of 3 acquired images in each case. B. Quantification of juxta-nuclear CHMP2A localisation during mitosis from A, quantification from 20 cells in interphase, prophase, pro-metaphase and metaphase, 23 cells in anaphase, 24 cells in telophase, 36 cells in early cytokinesis and 20 cells in late cytokinesis. C. HeLa cells stained with DAPI, anti-CHMP2A or anti-CHMP2B and either stably expressing YFP-LAP2β, or stained with anti-LBR. Arrows indicate regions of colocalisation. Scale bar is 10 μm, images representative of 2 (anti-CHMP2B and YFP-LAP2β, anti-LBR and anti-CHMP2A) or 4 (anti-CHMP2A and YFP-LAP2β) acquired images. D. Tomographic slices of HeLa cells stained with fluoronanogold anti-CHMP2A. Correlation depicted in Extended Data Figure 2A-2C,

arrow indicates nucleocytoplasmic channel, scale bar is 200 nm, image representative of 25 gold-decorated nucleocytoplasmic channels and quantified in Extended Data Figure 2H. E. Schematic depicting topological equivalence between annular fusion of the NE and ESCRT-dependent membrane fusion events.

Figure 2 : Classical ESCRT-interactions govern CHMP2A telophase-NE localisation

A. Immunofluorescence and quantification of NE localisation in HeLa cells transfected with the indicated siRNA and stained with anti-CHMP2A, anti-tubulin and DAPI (Number of cells scored from 4 independent experiments: Control, 58; CHMP4A, 59; CHMP4B, 55; CHMP4C, 53; CHMP3, 64; CHMP1A, 47; CHMP1B 52; CHMP2B, 44. Percentage NE localisation given ± S.D. * P = 0.014, ** P = 0.0004 (2-tailed Student's T-test), Scale bar is 10 μm, images representative of 47 cells (Control), 26 cells (CHMP4B siRNA) and 42 cells (CHMP3 siRNA). B. Western blotting of lysates from siRNA-depleted HeLa cells stably expressing mCherry-tubulin and the indicated $CHMP2A^{R}$-FLAG with anti-FLAG, anti-CHMP2A or anti-GAPDH antisera. C. Immunofluorescence of $CHMP2A^{R}$-FLAG recruitment to the telophase NE in CHMP2A-depleted cells. Scale bar is 10 μm, quantification in Extended Data Figure 4A, images representative of 30 cells (Control), 26 cells (L4D/F5D), 30 cells (RRR-AAA) and 26 cells (L216D/L219D).

Figure 3 : UFD1 directs NE-localisation of CHMP2A

A. β-galactosidase activity of yeast co-transformed with the indicated Gal4 and VP16 fused proteins (n = 3 ± S.D.). B. MST experiments displaying interaction of HIS-UFD1 with CHMP2A (Fraction unbound displayed, n = 5 ± S.D.) C, D. Immunofluorescence (D) and quantification of NE localisation (C: Control, 35 cells; UFD1-1, 42 cells; UFD1-2, 25 cells; UFD1-3, 39 cells; average ± S.D. presented from 4 independent experiments) in HeLa cells transfected with the indicated siRNA and stained with anti-CHMP2A, anti-tubulin and DAPI, scale bar is 10 μm, images representative of 23 cells (Control), 34 cells (UFD1-1) 14 cells (UFD1-2) and 24 cells (UFD1-3).

Figure 4: ESCRT-III depletion disrupts nuclear envelope integrity

A. Timelapse analysis of NE-sealing in siRNA transfected HeLa cells stably expressing H2B-mCh and GFP-NLS-βGal. GFP-signal presented according to pseudocolour scale at the indicated timepoints. Scale bar is 10 μm, a single image was pseudocoloured for demonstrative purposes. B. Quantification of NE-sealing from siRNA treated cells as in A, (Cells were quantified at each time point; Ctrl 140 cells from 7 independent experiments; CHMP2A-1, 98 cells from 5 independent experiments, P = 0.047; CHMP2A-2, 80 cells from 4 independent experiments, P = 0.023; CHMP2A + CHMP2B, 60 cells from 3 independent experiments, P = 0.006; CHMP3, 34 cells from 3 independent experiments, P = 0.002. All values quoted ± S.E.M.; 2-tailed Student's t-test used to assess significance after 85 minutes). C. Western blotting of cell lysates from B with anti-CHMP2A, anti-CHMP2B anti-CHMP3 or anti-GAPDH antisera. D. Z-slices extracted from a correlative tomographic reconstruction of the NE at 60 minutes post anaphase onset from the indicated

siRNA-transfected mCh-Tub HeLa cells. The numbered circles correspond to discontinuities labeled in the 3D reconstructions in Extended Data Figure 10A, scale bar is 200 nm, image representative of 6 (control) and 12 (CHMP2A-1 siRNA) tomographic reconstructions. E. The percentage of discontinuities smaller than 65 nm was scored. Discontinuities in this range that were not NPCs as a percentage of total discontinuities (including NPCs) for n number of reconstructed tomograms: Control 9.4 ± 3.0, n = 6; CHMP2A-1, 29.9 ± 4.7, P = 0.01, n = 12; CHMP2A-2, 28.3 ± 2.0, P = 0.021, n = 2. The increase in the percentage of non-NPC discontinuities was assessed by 2-tailed Student's T-test (average diameter of non-NPC discontinuities was 38 ± 22 nm (CHMP2A-1) and 58 ± 19 nm (CHMP2A-2)). F. Western blotting of lysates from siRNA-treated HeLa cells stably expressing H2B-mCh, GFP-NLS-βGal and siRNA-resistant CHMP2A^{R}-FLAG with anti-CHMP2A, anti-FLAG or anti-GAPDH antisera. G. Quantification of NE-sealing from cells treated with siRNA as in F and imaged from 4 independent experiments, (Mean nucleo-cytoplasmic ratio given 85 minutes post anaphase onset ± S.D, 2-tailed Student's T-test was used to assess significance across 4 independent experiments (*); Ctrl, 8.9 ± 3.1, n = 174 ; CHMP2A siRNA 5.4 ± 2.6, n = 171, P = 0.0006; CHMP2A siRNA + CHMP2A^{R}-FLAG 8.4 ± 3.3, n = 132, not-significant; CHMP2A siRNA + CHMP2A^{R}-FLAG RRR-AAA 5.4 ± 2.2, n = 196, P = 0.0001).

References

1. Burke, B. The nuclear envelope: filling in gaps. *Nat. Cell Biol.* **3,** E273–4 (2001).
2. Anderson, D. J. & Hetzer, M. W. Shaping the endoplasmic reticulum into the nuclear envelope. *J. Cell. Sci.* **121,** 137–142 (2008).
3. Schooley, A., Vollmer, B. & Antonin, W. Building a nuclear envelope at the end of mitosis: coordinating membrane reorganization, nuclear pore complex assembly, and chromatin de-condensation. *Chromosoma* **121,** 539–554 (2012).
4. Burke, B. & Ellenberg, J. Remodelling the walls of the nucleus. *Nat. Rev. Mol. Cell Biol.* **3,** 487–497 (2002).
5. Lu, L., Ladinsky, M. S. & Kirchhausen, T. Formation of the postmitotic nuclear envelope from extended ER cisternae precedes nuclear pore assembly. *J. Cell Biol.* **194,** 425–440 (2011).
6. Hetzer, M. *et al.* Distinct AAA-ATPase p97 complexes function in discrete steps of nuclear assembly. *Nat. Cell Biol.* **3,** 1086–1091 (2001).
7. McCullough, J., Colf, L. A. & Sundquist, W. I. Membrane Fission Reactions of the Mammalian ESCRT Pathway. *Annu. Rev. Biochem.* (2013). doi:10.1146/annurev-biochem-072909-101058
8. Carlton, J. G., Agromayor, M. & Martin-Serrano, J. Differential requirements for Alix and ESCRT-III in cytokinesis and HIV-1 release. *Proc. Natl. Acad. Sci. U.S.A.* **105,** 10541–10546 (2008).
9. Carlton, J. G. & Martin-Serrano, J. Parallels between cytokinesis and retroviral budding: a role for the ESCRT machinery. *Science* **316,** 1908–1912 (2007).
10. Elia, N., Sougrat, R., Spurlin, T. A., Hurley, J. H. & Lippincott-Schwartz, J. Dynamics of endosomal sorting complex required for transport (ESCRT) machinery during cytokinesis and its role in abscission. *Proc. Natl. Acad. Sci. U.S.A.* **108,** 4846–4851 (2011).
11. Morita, E. *et al.* Human ESCRT and ALIX proteins interact with proteins of the midbody and function in cytokinesis. *EMBO J.* **26,** 4215–4227 (2007).
12. Jouvenet, N., Zhadina, M., Bieniasz, P. D. & Simon, S. M. Dynamics of ESCRT protein recruitment during retroviral assembly. *Nat. Cell Biol.* **13,** 394–401 (2011).
13. Carlton, J. G., Caballe, A., Agromayor, M., Kloc, M. & Martin-Serrano, J. ESCRT-III governs the Aurora B-mediated abscission checkpoint through CHMP4C. *Science* **336,** 220–225 (2012).
14. Clever, M., Funakoshi, T., Mimura, Y., Takagi, M. & Imamoto, N. The nucleoporin ELYS/Mel28 regulates nuclear envelope subdomain formation in HeLa cells. *Nucleus* **3,** 187–199 (2012).
15. Stauffer, D. R., Howard, T. L., Nyun, T. & Hollenberg, S. M. CHMP1 is a novel nuclear matrix protein affecting chromatin structure and cell-cycle progression. *J. Cell. Sci.* **114,** 2383–2393 (2001).
16. Morita, E. *et al.* ESCRT-III protein requirements for HIV-1 budding. *Cell Host Microbe* **9,** 235–242 (2011).
17. Morita, E. *et al.* Human ESCRT-III and VPS4 proteins are required for centrosome and spindle maintenance. *Proc. Natl. Acad. Sci. U.S.A.* **107,** 12889–12894 (2010).
18. Asencio, C. *et al.* Coordination of kinase and phosphatase activities by Lem4 enables nuclear envelope reassembly during mitosis. *Cell* **150,** 122–135 (2012).
19. Buchkovich, N. J., Henne, W. M., Tang, S. & Emr, S. D. Essential N-terminal insertion motif anchors the ESCRT-III filament during MVB vesicle formation. *Dev. Cell* **27,** 201–214 (2013).
20. Ramadan, K. *et al.* Cdc48/p97 promotes reformation of the nucleus by extracting the kinase Aurora B from chromatin. *Nature* **450,** 1258–1262 (2007).
21. Dobrynin, G. *et al.* Cdc48/p97-Ufd1-Npl4 antagonizes Aurora B during chromosome segregation in HeLa cells. *J. Cell. Sci.* **124,** 1571–1580 (2011).
22. Ritz, D. *et al.* Endolysosomal sorting of ubiquitylated caveolin-1 is regulated by VCP and UBXD1 and impaired by VCP disease mutations. *Nat. Cell Biol.* **13,** 1116–1123 (2011).
23. Anderson, D. J. & Hetzer, M. W. Reshaping of the endoplasmic reticulum limits the rate for nuclear envelope formation. *J. Cell Biol.* **182,** 911–924 (2008).
24. Sorg, G. & Stamminger, T. Mapping of nuclear localization signals by simultaneous fusion to green fluorescent protein and to beta-galactosidase. *BioTechniques* **26,** 858–862 (1999).
25. Lee, C.-P. *et al.* The ESCRT machinery is recruited by the viral BFRF1 protein to the nucleus-associated membrane for the maturation of Epstein-Barr Virus. *PLoS Pathog.* **8,** e1002904 (2012).
26. Pawliczek, T. & Crump, C. M. Herpes simplex virus type 1 production requires a functional ESCRT-III complex but is independent of TSG101 and ALIX expression. *J. Virol.* **83,** 11254–11264 (2009).

27. Speese, S. D. *et al.* Nuclear envelope budding enables large ribonucleoprotein particle export during synaptic Wnt signaling. *Cell* **149,** 832–846 (2012).
28. Webster, B. M., Colombi, P., Jäger, J. & Lusk, C. P. Surveillance of Nuclear Pore Complex Assembly by ESCRT-III/Vps4. *Cell* **159,** 388–401 (2014).

Online Supplementary Information

Online Methods

Cell Culture

HeLa and 293T cells were kind gifts from Prof Juan Martin-Serrano (KCL) and were cultured in DMEM containing 10% FBS, Penicillin (100U/ml) and Streptomycin (0.1 mg/ml). GP2-293 cells were obtained from Clontech and were cultured similarly. BJ fibroblasts were obtained from the ATCC and cultured in 4:1 DMEM : 199 Media, supplemented with 15% FCS, Penicillin (100U/ml) and Streptomycin (0.1 mg/ml). Stable cells lines were generated by transduction using MLV-based retroviruses as described previously[9], and selected using Puromycin (200 ng/ml), G418 (500 μg/ml) or hygromycin (200 μg/ml) as necessary. Cells were sorted to monoclonality by limiting dilution or FACS. HeLa cells stably expressing mCh-Tubulin[29] or GFP-CHMP4B[12] have been described previously and were kind gifts from Prof Juan Martin-Serrano (KCL). MycoSensor (Agilent) was used to screen for contamination.

Plasmids

Plasmids encoding TSG101, EAP20, EAP30, EAP45, CHMP1A, CHMP1B, CHMP2A, CHMP2B, CHMP3, CHMP4A, CHMP4B, CHMP4C, CHMP5, VPS4A, LIP5, UBPY, CEP55, TAL, LAP2β and ALG2 were kind gifts from Prof. Juan Martin-Serrano (King's College London) and have been described previously[8,9,13,30]. Coding sequences for p97, p47, NPL4, UFD1, CHMP7, VPS4B and SPARTIN were amplified from IMAGE clones (6502535, 3635947, 5017718, 3507963, 5551762, 6042862, 5313378) respectively and were cloned into mammalian expression (pCR3.1-YFP) and yeast 2-hybrid plasmids (pHB18 and pGBKT7). A plasmid encoding HD-PTP was a kind gift from Prof Phillip Woodman (University of Manchester) and was cloned similarly. siRNA resistant CHMP2A constructs were created by introducing Q132Q, A133A, E134E, I135I, and D137D silent mutations in the CHMP2A coding sequence by PCR. 5' EcoRI and 3' NotI sites were added to facilitate cloning. Additional CHMP2A truncations, mutations and deletions were created by standard PCR procedures. UFD1 and its deletions were cloned with 5' and 3' NotI sites into relevant expression vectors. CHMP2A constructs were subcloned into pGBKT7 and UFD1 constructs were cloned into pHB18 for yeast 2-hybrid analysis. For recombinant protein expression, CHMP2A was cloned into pGEX-EcoRI-NotIXhoI and UFD1 constructs were cloned into pET28a (kind gifts from Prof Juan Martin-Serrano). A lentiviral expression vector (pLVXP) was a kind gift from Dr Mark Dodding (KCL) and modified to express a GFP-EcoRI-NotI-XhoI polylinker by replacing its SnaBI/XbaI fragment with a GFP-EcoRI-XhoI-NotI-STOP-XbaI fragment, obtained by PCR from pCR3.1-GFP-EcoRI-XhoI-NotI (a kind gift from Prof Juan Martin-Serrano, KCL). SnaBI/XhoI fragments of pHM840 (encoding GFP-NLS-βGAL and obtained from Thomas Stamminger (Universitätsklinikum Erlangen) via Addgene)

were cloned into the SnaBI/XhoI sites of pLVXP-GFP-ENX to produce pLVXP-GFP-NLS-βGAL. pLVXP-GFP-NLS was obtained by amplifying GFP using primers to incorporate a C-terminal SV40 NLS.

A SnaBI/NotI fragment from pH2B-mCherry-IRES-Neo3 (a kind gift from Dr Ulrike Eggert (King's College London)) was subcloned into SnaBI/Not sites of pLHCX-MCS (a modified version of pLHCX containing a HindIII/MluI/SalI/XhoI/NotI/HpaI/BamHI/NsiI/ClaI MCS, a kind gift from Prof T. Ng, King's College London) to create pLHCX-H2B-mCh. LAP2β residues 244-454 were amplified with in-frame NotI sites and cloned into the NotI site of pMSCVneo-YFP-EXN to create pMSCVneo-YFP-LAP2β. siRNA-resistant CHMP2A constructs were cloned with C-terminal FLAG extensions into EcoRI and NotI sites of pCR3.1-EXN and subcloned into pNG72-ENX (kind gifts from Prof Juan Martin-Serrano).

For retroviral transduction, above constructs within pMSCVneoYFP-EXN, pNG72 pLHCX-MCS retroviral packaging vectors were transfected with pVSVG into 293GP2 cells (all from Clontech). Supernatants were harvested, clarified by centrifugation (200 x g, 5 minutes), filtered (0.45 μm) and used to infect target cells in the presence of 8μg/ml polybrene (Millipore) at MOI < 1. For lentiviral transduction, 293T cells were transfected with pCMV8.91, pVSVG and either pLVXP-GFP-NLS-βGAL, pLVXP-GFP-NLS-PK or pLVXP-GFP-NLS. Supernatants were harvested, clarified by centrifugation (200 x g, 5 minutes), filtered (0.45 μm) and used to infect target cells in the presence of 8μg/ml polybrene (Millipore) at MOI < 1. In both cases, antibiotic selection was applied after 48 hours.

Antibodies

Antibodies against HSP90 (H114) were from Santa Cruz Biotechnology, TSG101 (T5701) was from Sigma, GAPDH (MAB374) was from Millipore, Tubulin (DM1A) was from Sigma, CHMP2A (104771-AP) was from Proteintech, CHMP2B (ab33174) was from Abcam, CHMP4B (sc82556) was from Santa Cruz, CHMP3 (sc67228) was from Santa Cruz, UFD1 (106151-AP) was from Proteintech, anti-p24 Gag (183-H12-5C) was from the NIH AIDS Research and Reference Reagent Program, EGFR (2232) was from Cell Signaling Technology, GFP (7.1/13.1) was from Roche, LBR (SAB10400151) was from Sigma, Lamin A/C (MAB3538) was from Millipore, mAb414 was from Covance, DYKDDDDK-Tag (FLAG) was from Cell Signaling Technology. Alexa conjugated secondary antibodies were from Invitrogen and HRP-conjugated secondary antibodies were from Millipore.

SDS-PAGE and western blotting

Cell lysates were denatured in Laemmli buffer and resolved using SDS-PAGE gels. Resolved proteins were transferred onto nitrocellulose by western blotting and were probed with the indicated antisera in 5% milk. HRP-conjugated secondary antibodies were incubated with ECL Prime enhanced chemiluminescent substrate (GE Healthcare) and visualized by exposure to autoradiography film.

Transient transfection of cDNA

HeLa cells were transfected using Lipofectamine-2000 (Life Technologies) according to the manufacturers instructions. 293GP2 and 293T cells were transfected using linear 25-kDa polyethylenimine (PEI, Polysciences, Inc.)

siRNA transfections

Cells were seeded at a density of 1E5 cells/ml (HeLa, BJ) or 2.6E5 cells/ml (293T) and were transfected with siRNA at 100nM, 2 hours after plating using Dharmafect-1 (Dharmacon). To minimize toxicity associated with CHMP2A and UFD1 depletion, single transfections were performed for 72 hours. The following targeting sequences that have already been demonstrated to achieve potent and specific suppression of the targeted CHMP were employed: Control – Dharmacon Non-targeting control D-001810-01. CHMP2A-1 : aggcagagaucauggauaudTdT[16], CHMP2A-2 : AAGAUGAAGAGGAGAGUGAdTdT[17], CHMP2B : UCGAGCAGCUUUAGAGAAAdTdT[17], CHMP3 ggaagaagcagaaauggaadTdT[17], CHMP4A Q-SI04268845[13], CHMP4B Q-SI00325199[13], CHMP4C Q-SI04279674[13], CHMP1A CCAAGAAGGCGGAGAAGGAdTdT[17], CHMP1B UGGACAAAUUCGAGCACCAdTdT[17], UFD1-1 GAGGCAGAUUCGUCGCUUUdTdT, UFD1-2 MQ-017918-03-0002, UFD1-3 GUGGCCACCUACUCCAAAUdTdT[31], LEM4 GAGAAGACGCUGAGAAAUUdTdT[18]. UFD1-2 was excluded from much of the analysis due to toxicity and morphological changes specific to this oligo.

Yeast Two-Hybrid assays

Yeast Y190 cells were co-transformed with plasmids encoding the indicated proteins fused to the VP16 activation domain (pHB18) or the Gal4 DNA-binding domain (pGBKT7). Co-transformants were selected on SD-Leu-Trp agar for 3 days at 30 ^{o}C, harvested, and *LacZ* activity was measured using a liquid β-galactosidase assay employing chlorophenolred-ß-D-galactopyranoside (Roche) as a substrate. Average β-galactosidase activities presented.

Lentiviral release

293T cells were transfected with siRNA as described above, except that the second transfection contained additionally either 300 ng of HIV-1 pCMVd8.91 (a kind gift from Prof T. Ng, King's College London), 100ng of pLenti-SEW (a packaging vector encoding GFP, a kind gift from Prof A. Ridley, King's College London) and 100 ng pVSVG. After 48 hours, virions were harvested from 293T supernatants by filtration (0.45 μm) and centrifugation through 20% sucrose (14000 rpm, 120 minutes), lysed, resolved by SDS-PAGE and examined by western blotting. Additionally, HeLa cells were infected with 50 μl of viral supernatant and GFP-expression in these cells was measured by western blotting. Virion Release was calculated by quantifying $Gag^{Virion}/Gag^{Cellular}$ as determined densitometry using ImageJ.

Co-Precipitation Assays

293T cells were co-transfected equal quantities of the indicated pCAGGS-GST construct and the relevant pCR3.1-YFP construct for 48 hours. Cells were harvested and lysed in 1 ml of 50 mM Tris·HCl, pH 7.4, 150 mM NaCl, 5 mM EDTA, 5% glycerol, 1% Triton X-100, a protease inhibitor mixture (complete mini-EDTA-free, Roche). Clarified lysates were incubated with glutathione-Sepharose beads (Amersham Biosciences) for 3 h at 4 °C and washed three times with wash buffer (50 mM Tris·HCl, pH 7.4, 150 mM NaCl, 5 mM EDTA, 5% glycerol, 0.1% Triton X-100). Bead-bound proteins were recovered in Laemmli sample buffer, resolved by SDS-PAGE and examined by western blotting.

Production of recombinant proteins

BL21* DE3 *E. coli* expressing plasmids encoding GST-tagged or HIS-tagged proteins were collected in bacterial lysis buffer (20mM Hepes (pH 7.4), 500 mM NaCl, supplemented with complete mini, EDTA-free protease inhibitor (Roche) and 1 mM PMSF; buffers for HIS-tagged protein purification were supplemented with 20mM Imidazole. Cells were lysed by addition of lysosyme (1 mg/ml, 15 minutes), Triton X100 (0.25%, 15 minutes) and were snap frozen in liquid nitrogen. Cells were thawed on ice, clarified through addition of DNAse1 (20 μg/ml) and soluble proteins were collected by centrifugation at 28000 x g for 30 minutes. Proteins were immobilised on Glutathione Sepharose 4β or Ni-NTA-sepharose resin, washed in wash buffer (20mM Hepes, pH7.4, 150mM NaCl), containing 20mM Imidazole if required. Proteins were eluted from Glutathione Sepharose 4β resin in wash-buffer supplemented with 10mM reduced Glutathione (pH 8), or were eluted from Ni-NTA sepharose with a step gradient of imidazole. CHMP2A was cleaved from the GST using AcTEV protease (Life Technologies). Protein concentrations were measured using the Qubit assay system (Life Technlogies).

Microscale thermophoresis (MST)

Measurements were preformed using a Monolith NT.115 instrument (Nanotemper). Briefly, recombinant CHMP2A was labeled with Alexa-647 using an NHS Amine-reactive labeling kit (Nanotemper), labeling was verified by infrared imaging (Licor). 360nM Alexa-647 CHMP2A was combined with serial dilutions of GST, HIS-UFD1 or HIS-UFD1 1-257 (maximally 52.8 μM). Interactions were performed in 150 mM NaCl, 20 mM Hepes, 0.04% Tween-20 pH 7.4. Temperature jump and thermophoresis experiments were conducted using 100% LED illumination and 40% IR laser power and were analysed using Nanotemper's analysis suite. Binding curves could only be generated for the CHMP2A : UFD1 interaction, affinities were calculated by the software and averaged.

Fixed cell imaging

Cells were imaged using Nikon Eclipse microscopes teamed with widefield (Ti-E) and confocal (A1R or

Spinning Disc) imaging systems. Widefield image stacks were iteratively deconvolved using Autoquant. Images were processed in NIS Elements and exported to Photoshop for assembly. HeLa cells were fixed in MeOH (for CHMP2A-staining) or 4% PFA and subject to processing for immunofluorescence as described previously[9]. For multinucleation and midbody arrest assays, at least 300 cells per experiment were quantified. For telophase NE localisation, at between 10 and 20 telophase cells per experiment were scored. For fixed cell microscopical analysis, we scanned multiple coverslips and experiments before acquiring two to three representative images for presentation in figures.

Live cell imaging

HeLa cells stably expressing the indicated proteins were plated in Stickyslides (Ibidi) adhered to a glass number 1 coverslip and transfected with the indicated siRNA. Cells were synchronised using a double thymidine block and 48 hours after siRNA transfection (10.5 hours after release from the second thymidine block), cells were transferred to a Nikon inverted spinning disc confocal microscope with attached environmental chamber and imaged live for 4 hours using a 20x dry objective and a 1.5 x magnification lens. For mitotic rim formation, 3 co-ordinates per condition were selected and frames were acquired every 1 min, rim formation was scored through manual analysis of individual frames. For nuclear accumulation of GFP-NLS and GFP-NLS-ßGal, frames were acquired every 1 min. The ratio of background-corrected, area-normalised, GFP-positive pixel intensities within the cytoplasm and mCh-H2B demarcated nuclei at the indicated intervals were obtained using NIS-elements. We excluded 2/98 cells from CHMP2A-1 analysis, 2/60 cells from UFD1-1 analysis and 2/60 cells from UFD1-3 analysis as these gave anomalous N/C ratios > 10 x S.D. from the average. For imaging of GFP-CHMP4B recruitment to the telophase NE, cells were imaged using a 100x oil-immersion objective and confocal slices were acquired every 30 seconds using a spinning disc confocal microscope. For analysis of nuclear retention, siRNA-treated HeLa cells stably expressing GFP-NLS and mCh-H2B were imaged live using a Nikon A1R confocal microscope. Between 1 and 2 hours post anaphase onset, cells were subject to photo-ablation of cytosolic GFP-NLS signal by point bleaching and the recovery of cytoplasmic fluorescence from the nuclear pool was quantified for 10 minutes post-bleach.

Correlative Light Electron Microscopy

500,000 HeLa cells were seeded in a 3.5cm Mattek gridded dish (P35G-2-14-C-GRID). The following morning, cells were fixed in phosphate buffer containing 1% PFA for 3 minutes. Cells were permeabilised with 0.1% saponin in PHEM (60mM PIPES, 25mM HEPES, 10mM EGTA, 2mM $MgCl_2$, pH6.9) and processed for immunofluorescence using anti-CHMP2A primary and goat anti-rabbit Alexa^{594}-conjugated fluoronanogold (Nanoprobes) and DAPI. Cells were subjected to a subsequent 10-minute 3% PFA fixation and quenching prior to imaging on a Leica SP5 or SP8 confocal microscope.

After fluorescent imaging, cells were postfixed in glutaraldehyde, subjected to silver enhancement (Aurion RGENT SE-EM), stained with OsO_4 and uranyl acetate, dehydrated through ethanol and embedded in Epon. Blocks were trimmed to the region identified by confocal imaging and 300 nm serial sections were cut using a diamond knife[32]. For retracing of the cells of interest sections were imaged on a FEI Tecnai12 and subsequently double tilt series of regions of interest were acquired on a FEI Tecnai20. Tilt series were reconstructed using iMOD and selected frames and movies were extracted using ImageJ.

For quantification of holes remaining in the NE after CHMP2A depletion, tomograms were acquired by CLEM as described above. Discontinuities in the NE were scored as being NPC or non-NPC on the basis of cross sectional morphology. Internal diameters of these discontinuities were measured from reconstructed tomograms using FIJI. Discontinuities were segregated by size and whether they were identifiable as NPCs or not. A threshold was set at 65 nm (> 2 S.D. smaller than the measured control NPC diameter) and the percentage of discontinuities smaller than this was displayed. At least 50 discontinuities were analysed per treatment across multiple cells from the indicated number of tomograms.

Statistical analysis

Variance wan analysed using an F-test and type-relevant 2-tailed Student's T-tests were used to assess significance between test samples and controls.

ImageStream Analysis

siRNA-treated HeLa cells in 6-well dishes were detached, fixed in 4% PFA, permeabilised with 0.1% Tx100 and stained in suspension with mAb414, Alexa^{594} conjugated secondary antibodies and DAPI (at 0.1 μg/ml). In-focus, single-cellular populations were acquired and a mask was applied to the DAPI channel and duplicated then dilated by 3 pixels to encompass the mAb414 signal surrounding the nuclei. The difference in mAb414 signal captured by these masks was given as the nuclear envelope mAb414 and presented as a histogram. Representative images of average mAb414 intensity were extracted for presentation.

Extended Data Figure Legends

Extended Data Figure 1 : Localisation of ESCRT components during the cell cycle

A, B. Immunofluorescence analysis of HeLa cells stained with anti-tubulin, anti-CHMP2A or -CHMP2B and DAPI (A). Images in A representative of 2 acquired images per field of view. Cells in B were treated with Control or CHMP2A-targeting siRNA, images representative of 4 acquired images (control) or 2 acquired images (CHMP2A siRNA). C. Deconvolved projections of HeLa cells stained with anti-CHMP2A and DAPI, corresponds to stills from Supplemental Video 1, images representative of 2 deconvolved image series. D. HeLa cells stably expressing GFP-CHMP4B were imaged live during the anaphase to telophase transition. Telophase frames at 30 second intervals are presented, corresponding to stills from Supplemental Video 2, images representative of 4 acquisitions. E. Immunofluorescence analysis of human diploid fibroblasts stained with anti-CHMP2A, anti-tubulin and DAPI, images representative of 3 acquired cells per cell cycle phase. F, G. Immunofluorescence analysis of HeLa cells stained with anti-CHMP2A, DAPI and either, anti-mAb414 (F) or anti-LaminA/C (G), images representative of 5 acquired cells. Arrowheads indicate regions of formed nuclear pores or lamina as indicated. H. Quantification of abnormal nuclei (the presence of multiple lobes, micronuclei, lamina ingression or invagination) in HeLa cells transfected with the indicated siRNA and stained with anti-LaminA/C (1300 cells over 5 experiments quantified per treatment ± S.D.). Images representative of 3 (control, CHMP2A siRNA) or 2 (LEM4 siRNA) acquired fields of view and resolved cell lysates were examined by western blotting with anti-CHMP2A, anti-CHMP2B or anti-GAPDH antisera as indicated. In all cases, scale bar is 10 μm.

Extended Data Figure 2 : Correlative light and electron microscopy of endogenous CHMP2A localisation in telophase NE

A-C. Phase contrast (A), correlative immunofluorescence (B, scale bar is 10 μm) and transmission electron microscopy of HeLa cells stained with anti-CHMP2A, detected by Alexa^{594}-fluoronanogold and DAPI. Boxed region in A is shown in B, boxed region in B is shown in C, in all cases, images representative of 3 cells prepared for CLEM. D. 3D rendering of tomographic reconstruction of forming NE from boxed region in C and Figure 1D, a single example of a nucleocytoplasmic channel was selected for 3D rendering. E-G. Z-slices extracted from tomographic reconstructions of forming NE depicting CHMP2A-localisation to isolated vesicles (Ei) and nucleo-cytoplasmic channels (arrows in Eii, F, G) at the indicated Z-heights, scale bar is 200 nm. Localisation of CHMP2A to nucleocytoplasmic channels was observed in 3 independent cells, data from a second cell are presented in Extended Data Figure 3. Note CHMP2A localisation to nucleocytoplasmic channels is distinct from nuclear pores (asterix in Extended Data Figure 2F). H. Quantification of CHMP2A labeling from 2 independently prepared cells, channels were defined as discontinuities up to 80 nm, and gaps were defined as discontinuities over 80 nm. Distances of the gold-particles from channels or gaps were measured on the tomograms in 3-dimensions and plotted as a

histogram. The majority (74.4%) of gold label was found within 150 nm of nucleo-cytoplasmic channels and the majority (70.6 %) of the gold label was found more than 150 nm from the larger gaps in the NE.

Extended Data Figure 3: Correlative light and electron microscopy of endogenous CHMP2A localisation in telophase NE

A-C. Phase contrast (A), correlative immunofluorescence (B) and transmission electron microscopy (C) of a second HeLa cell stained with anti-CHMP2A, detected by Alexa^{594}-fluoronanogold and DAPI. Boxed region in A is shown in B, boxed region in B is shown in C. D. Z-slices extracted from tomographic reconstruction of forming NE from boxed region in C depicting CHMP2A-localisation to nucleo-cytoplasmic channels at the indicated Z-heights. Arrow indicates nucleocytoplasmic channel, scale bar is 200 nm, images in all cases representative of 3 cells processed for CLEM, quantification of gold localisation given in Extended Data Figure 2H.

Extended Data Figure 4 : Mitotic defects in cells reliant on mutated forms of CHMP2A

A. Quantification of CHMP2A recruitment to the telophase NE or the midbody from Figure 2C (n = 3 ± S.D., 10 cells (midbody or telophase) scored per experiment). B. Quantification of cytokinetic failure from cells treated with the indicated siRNA (300 cells were quantified per experiment, from 3 independent experiments ± S.D.).

Extended Data Figure 5 : Screening for ESCRT : p97 complex interactions

A-D. β-galactosidase activity of yeast co-transformed with the indicated Gal4 (ESCRT) and VP16 fused proteins (n = 2). E. Resolved cell lysates and glutathione-bound fractions from 293T cells transfected with the indicated fusion proteins were examined by western blotting with anti-GFP (n = 3). F. β-galactosidase activity of yeast co-transformed with the indicated Gal4 and VP16 fused proteins (n = 3 ± S.D.). G. MST experiments detailing binding of CHMP2A to GST (n = 4), HIS-UFD1 (n = 5) or HIS-UFD1 1-257 (n = 4, ± S.D.). As no reduction in thermophoresis signal was observed for GST or His-UFD1 1-257 across the concentration range, we present here the average thermophoresis signal change at equivalent protein concentrations for these three proteins, normalized to zero at the concentration in capillary 1. H. CHMP2A^{647}, HIS-UFD1 and HIS-UFD1 1-257 were examined by IR imaging or coomassie staining.

Extended Data Figure 6: UFD1 depletion does not effect ESCRT-dependent receptor degradation, lentivirus release or cytokinetic abscission

A. Resolved cell lysates of HeLa cells transfected with the indicated siRNA were examined by western blotting with anti-UFD1 or anti-HSP90 antisera. B. Resolved lysates of human diploid fibroblasts transfected with the indicted siRNA and treated for the indicated times with epidermal growth factor (20 ng/ml) were examined by western blotting with anti-EGFR, anti-UFD1 and anti-GAPDH antisera. EGFR

degradation was quantified by densitometry (n = 3, ± S.D.). C. Resolved cell lysates from 293T cells transfected with the indicated HIV-1 based lentiviral plasmids, a virally packaged GFP-plasmid, and the indicted siRNA were examined by western blotting with anti-p24 capsid, -HSP90, -TSG101, -CHMP2A, -CHMP2B and –UFD1 antibodies. Viral supernatants were collected and used to infect target HeLa cells. Resolved virions present in the 293T supernatant were examined by western blotting with anti-p24 capsid. Resolved lysates of infected HeLa cells were examined by western blotting with anti-GFP. Virion release was the ratio of released to cellular p24-capsid, as quantified by densitometry (n = 2); infectivity was quantified as GFP-signal in target cells, as quantified by densitometry (n = 2). D, siRNA-transfected HeLa cells were fixed and stained with anti-Tubulin. Multinucleate cells (n = 5, ± S.D.) or cells connected by midbodies (n = 5, ± S.D.) were scored visually, 300 cells scored per experiment.

Extended Data Figure 7: ESCRT-depletion impairs NE-rim formation.

A,B. Timelapse microscopy analysis and quantification of NE-rim formation in HeLa cells stably expressing YFP-LAP2β and mCh-H2B and treated with the indicated siRNA Scale bar is 10 μm. Time for rim formation post anaphase onset given (mins) (Ctrl 8.53 ± 0.09, 226 cells analysed over 8 independent experiments; CHMP2A-1, 7.60 ± 0.09, 205 cells analysed over 7 independent experiments; CHMP2A-2, 6.86 ± 0.12, 37 cells analysed over 2 independent experiments; CHMP2B, 6.92 ± 0.09, 79 cells analysed over 4 independent experiments; CHMP2A and CHMP2B, 6.84 ± 0.13, 50 cells analysed over 2 independent experiments; CHMP4B, 7.07 ± 0.14, 44 cells analysed over 2 independent experiments; UFD1 9.2 ± 0.18, 39 cells analysed over 3 independent experiments. All times mean ± S.E.M, in minutes, images representative of the indicated number of cell analysed). C. Resolved cell lysates from A were analysed by western-blotting with the indicated antisera.

Extended Data Figure 8: ESCRT-depletion does not impair nuclear pore formation.

A. Schematic of nuclear envelope integrity assay. B. Control siRNA treated HeLa cells reporting nucleo-cytoplasmic partitioning using the GFP-NLS-βGal assay, average NE compartmentalisation from 20 cells presented. Nucleo-cytoplasmic partitioning stabilises at 85 minutes (indicated by arrow). C. Immunofluorescence analysis of HeLa cells stably expressing YFP-LAP2β, transfected with the indicated siRNA then stained with anti-mAb414 and DAPI (n = 3), Scale bar is 10 μm. D. Mask employed to quantify nuclear pore formation by image-based flowcytometry (Imagestream). E. Imagestream analysis of HeLa cells transfected with the indicated siRNA, then stained with anti-mAb414 and DAPI. Nuclear pore intensity quantified by mask described in D. Representative images from 2 independent experiments, histogram and population averages displayed, graphical quantification of NPC intensity from the indicated number of gated cells (Control, 3045; CHMP2A-1, 1256; CHMP2A-2, 2152; CHMP2B, 5237; UFD1-1, 4146; UFD1-3, 4325; error bars are ± S.D.).

Extended Data Figure 9: Requirements for nucleocytoplasmic compartmentalization.

A. Quantification of NE-sealing from siRNA treated cells as in Figure 4B, (Ctrl 140 cells from 7 independent experiments; UFD1-1, 60 cells from 3 independent experiments, P = 0.044; UFD1-3, 60 cells from 3 independent experiments, P = 0.021; CHMP2B 40 cells from 2 independent experiments, N.S. All times quoted ± S.E.M. in minutes; 2-tailed student's T-test was used to assess significance at the 85-minute timepoint). B. Resolved cell lysates from A were analysed by western-blotting with the indicated antisera. C. Nuclear envelope integrity assay as performed with cells stably expressing mCh-H2B and GFP-NLS and transfected with the indicated siRNA. Differences in nucleo-cytoplasmic partitioning was assessed after plateau at the 65 minute timepoint using a 2-tailed Student's T-test : (Ctrl, 79 cells from 4 independent experiments, CHMP2A-1, 60 cells from 3 independent experiments, P = 0.048; CHMP2A-2, 52 cells from 3 independent experiments, P = 0.011; CHMP3, 28 cells from 3 independent experiments, P = 0.028, error bars represent S.E.M.). D, E. HeLa cells stably expressing mCh-H2B and GFP-NLS were transfected with the indicated siRNA and imaged live. 60 minutes post anaphase onset, cytoplasmic signal was photo-ablated (T = 0) and Recovery of cytoplasmic signal from the nuclear pool was calculated for the indicated conditions (Cytoplasmic : Nuclear ratio of GFP-NLS was normalized to T = 0. Ctrl, 21 cells from 4 independent experiments; CHMP2A-1, 24 cells from 4 independent experiments, P = 0.04; CHMP2A-2, 23 cells from 4 independent experiments, P = 0.05; CHMP3, 15 cells from 3 independent experiments, P = 0.004, 2-tailed Student's t-test was used to assess significance after 10 minutes. In D, error bars represent S.E.M. in E, scale bar is 10 μm. F. Scoring of multinucleate and midbody-connected HeLa cells transfected with the indicated siRNA and stained with anti-tubulin and DAPI (300 cells analysed per condition, n = 4 ± S.D.).

Extended Data Figure 10. Affect of CHMP2A depletion on NE discontinuities.

A. Presentation of reconstructed tomograms from Figure 4D. B. CHMP2A-depelted cells exhibited more non-NPC discontinuities per unit area whilst the number of NPC per unit area was constant, tomograms as described in Figure 4E were scored for discontinuities. The internal diameter of NPCs was slightly reduced in CHMP2A-depleted cells (Control 84 ± 7.6 nm, CHMP2A-1, 74 ± 8.8 nm; CHMP2A-2, 74 ± 5.7 nm). C. Schematic depicting topological equivalent of ESCRT-III-dependent membrane fusion events.

Supplementary Video 1 : CHMP2A forms a reticular network around telophase nuclei

Deconvolved 3D reconstruction of HeLa cells stained with anti-CHMP2A and DAPI and analysed by widefield microscopy, from Extended Data Figure 1C.

Supplementary Video 2 : GFP-CHMP4B transiently localises to telophase nuclei

Movie of GFP-CHMP4B localisation during the anaphase to telophase transition, from Extended Data Figure 1D.

Supplementary Video 3 : CHMP2A decorates nucleo-cytoplasmic channels

3D reconstruction of HeLa cells stained with anti-CHMP2A and DAPI and analysed by correlative light and electron tomography, From Figure 1D.

Supplementary Video 4 : Tomographic reconstruction of nascent nuclear envelope

3D reconstruction of HeLa cells stained with anti-CHMP2A and DAPI and analysed by correlative light and electron tomography, as depicted in Figure 1D and Extended Data Figure 2.

Supplemental References

29. Agromayor, M. *et al.* Essential role of hIST1 in cytokinesis. *Mol. Biol. Cell* **20,** 1374–1387 (2009).
30. Martin-Serrano, J., Yarovoy, A., Perez-Caballero, D., Bieniasz, P. D. & Yaravoy, A. Divergent retroviral late-budding domains recruit vacuolar protein sorting factors by using alternative adaptor proteins. *Proc. Natl. Acad. Sci. U.S.A.* **100,** 12414–12419 (2003).
31. Meerang, M. *et al.* The ubiquitin-selective segregase VCP/p97 orchestrates the response to DNA double-strand breaks. *Nat. Cell Biol.* **13,** 1376–1382 (2011).
32. van Weering, J. R. T. *et al.* Intracellular membrane traffic at high resolution. *Methods Cell Biol.* **96,** 619–648 (2010).

Olmos et al., Figure 1

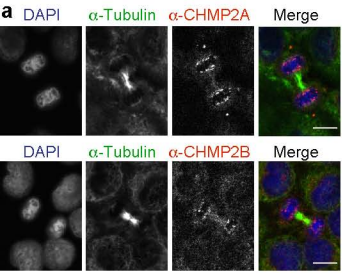

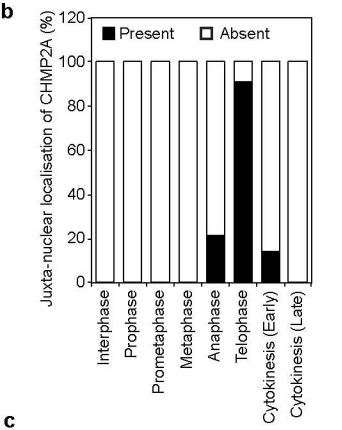

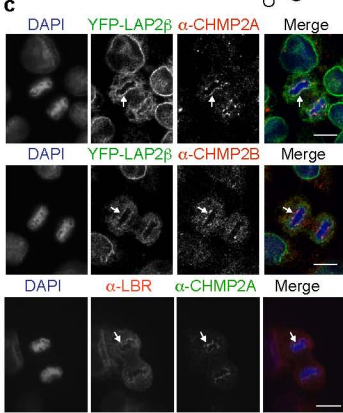

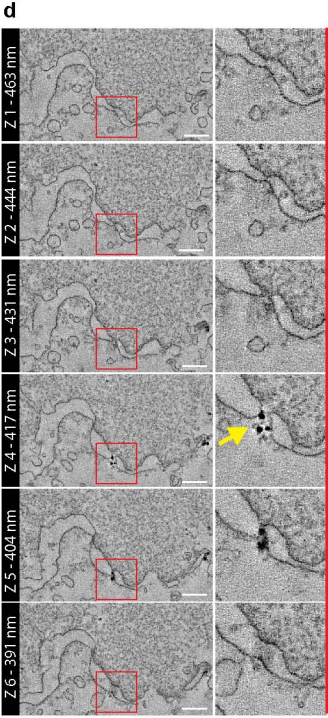

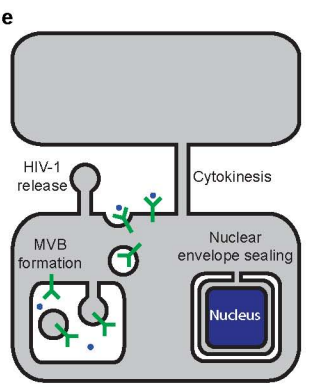

Olmos et al., Figure 2

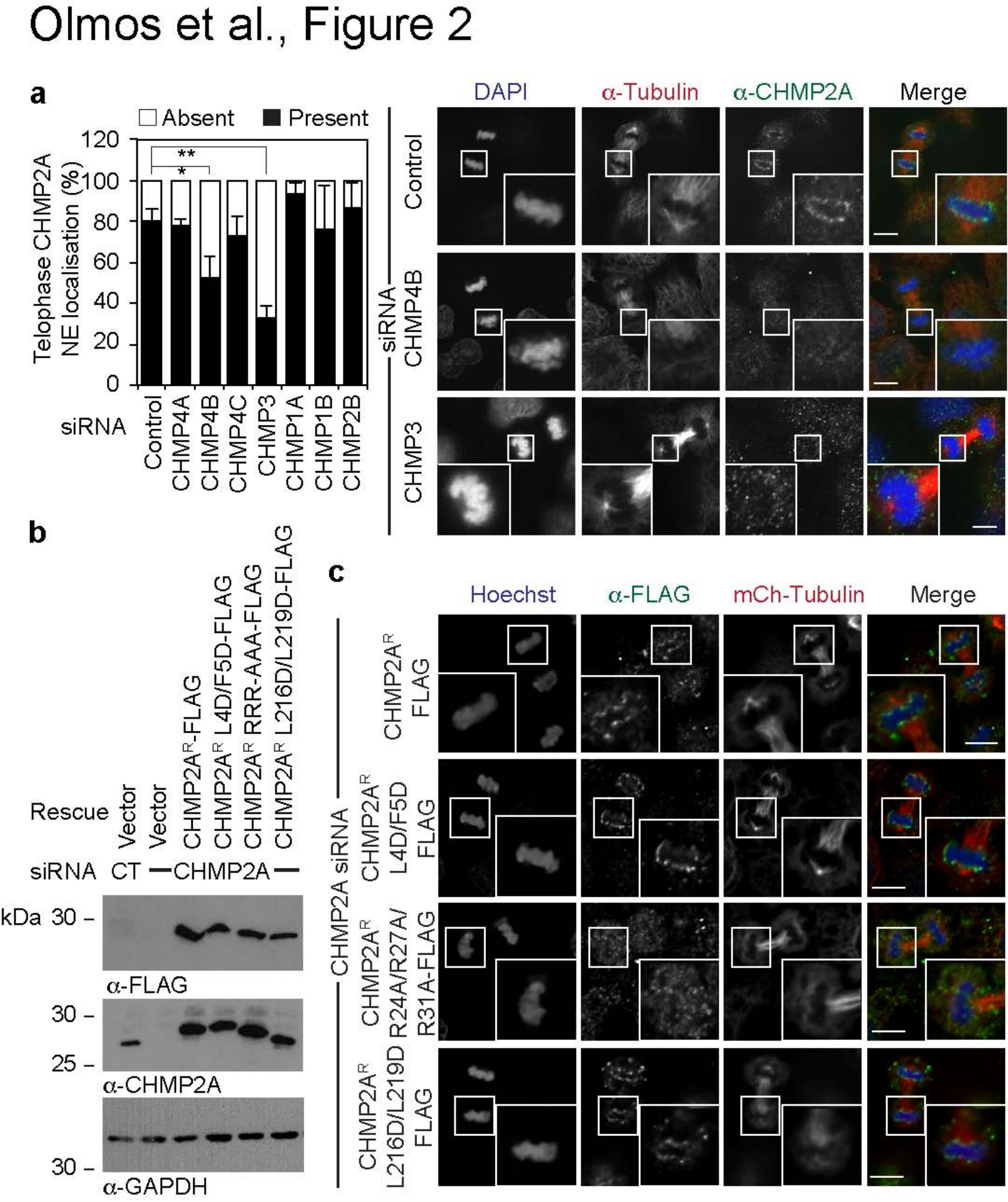

Olmos et al., Figure 3

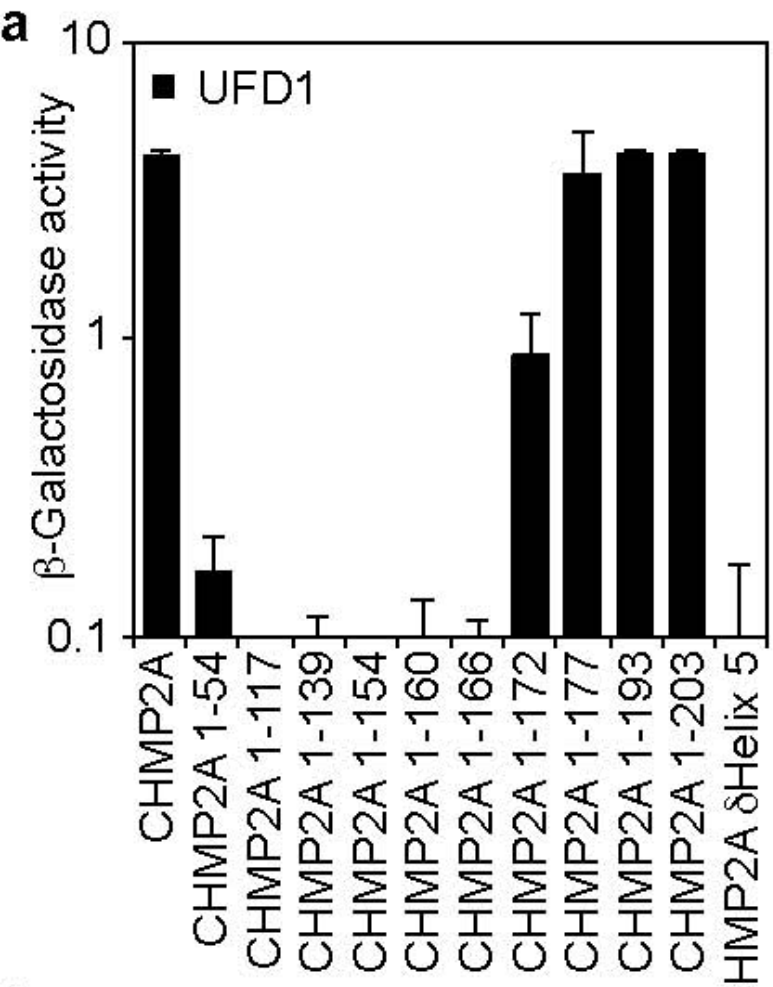

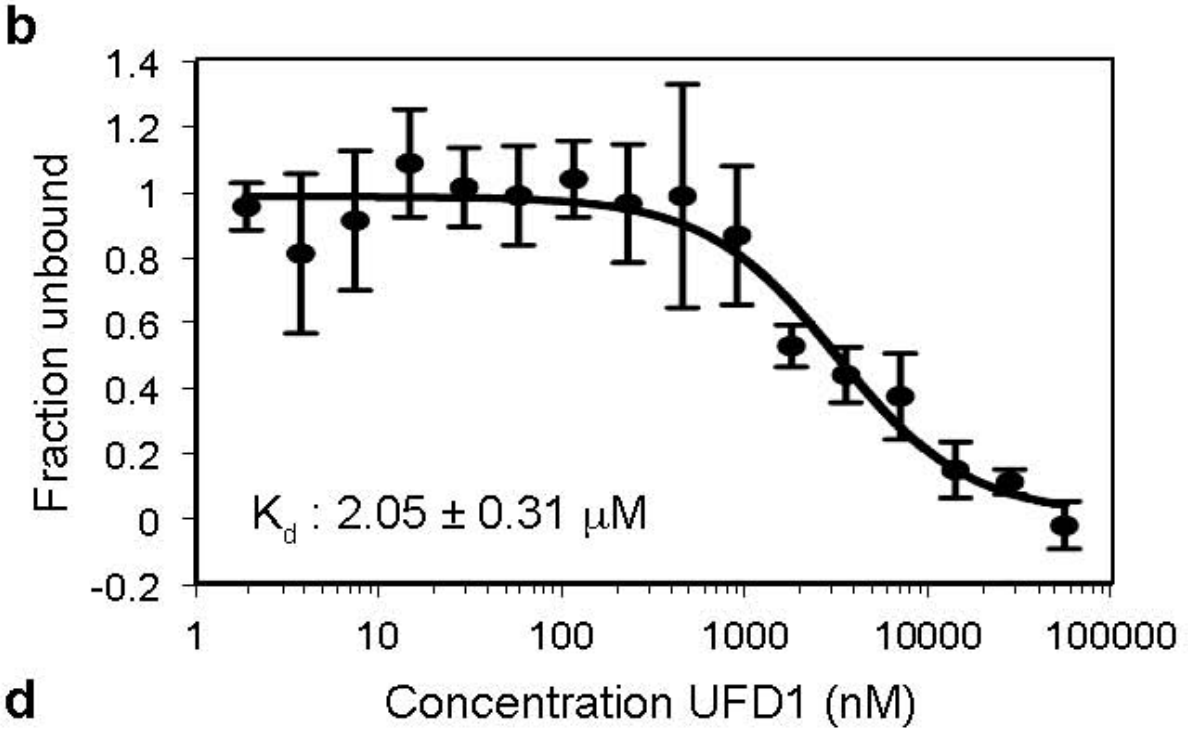

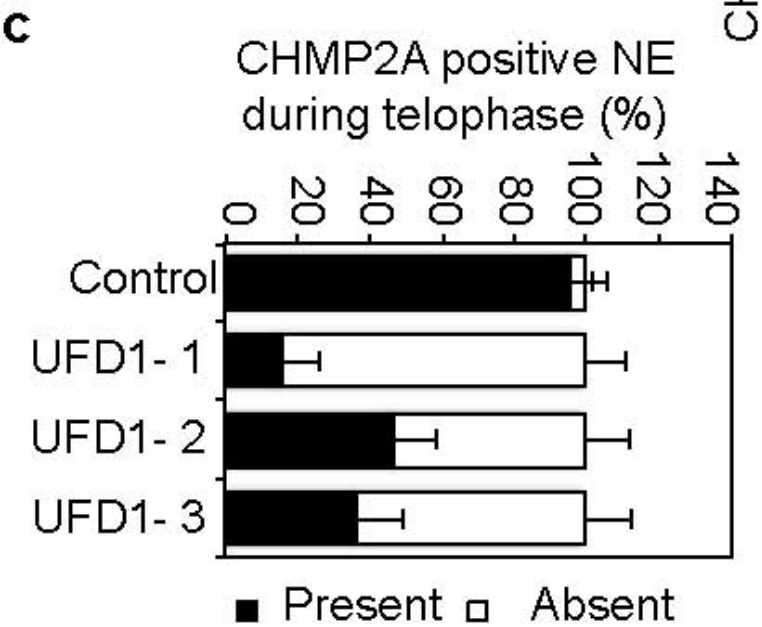

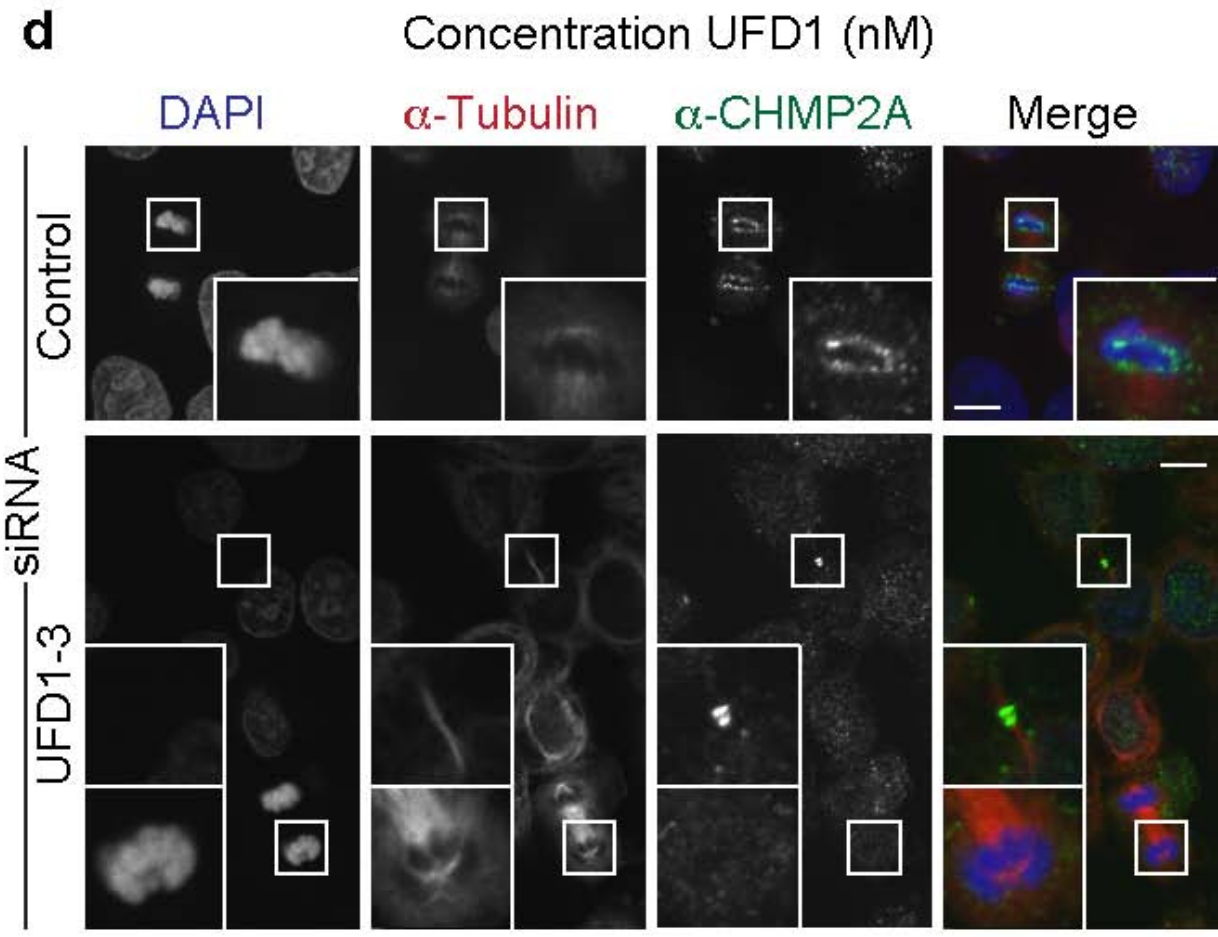

Olmos et al., Figure 4

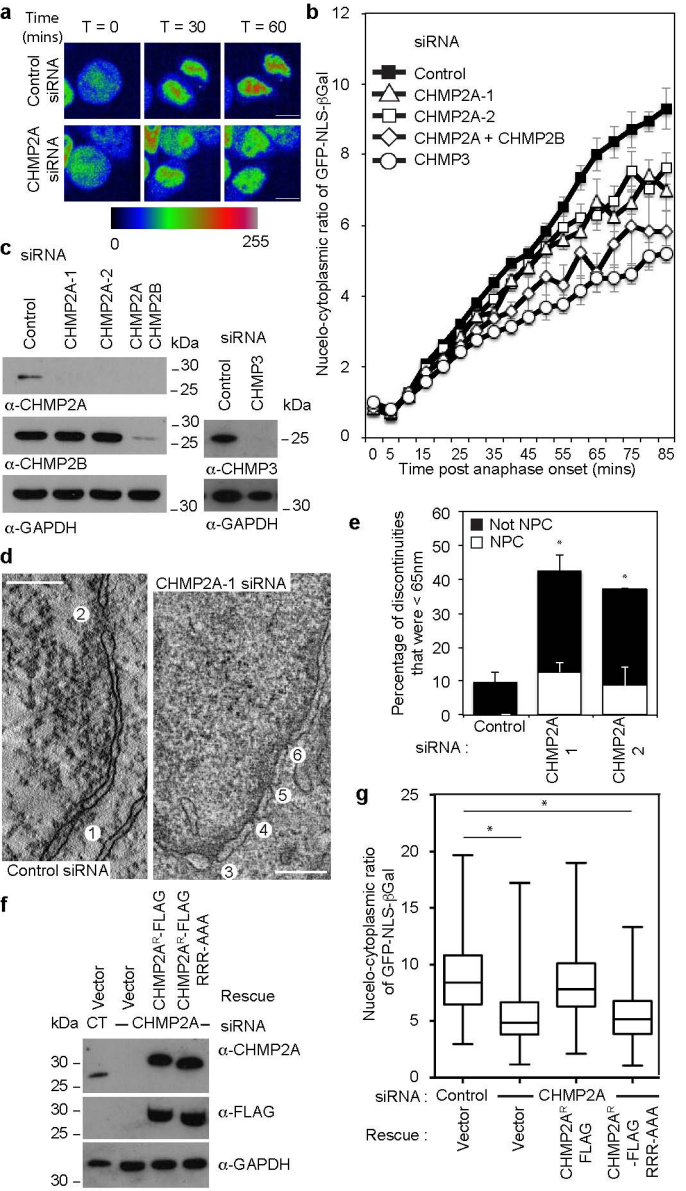

Olmos et al., ED Figure 1

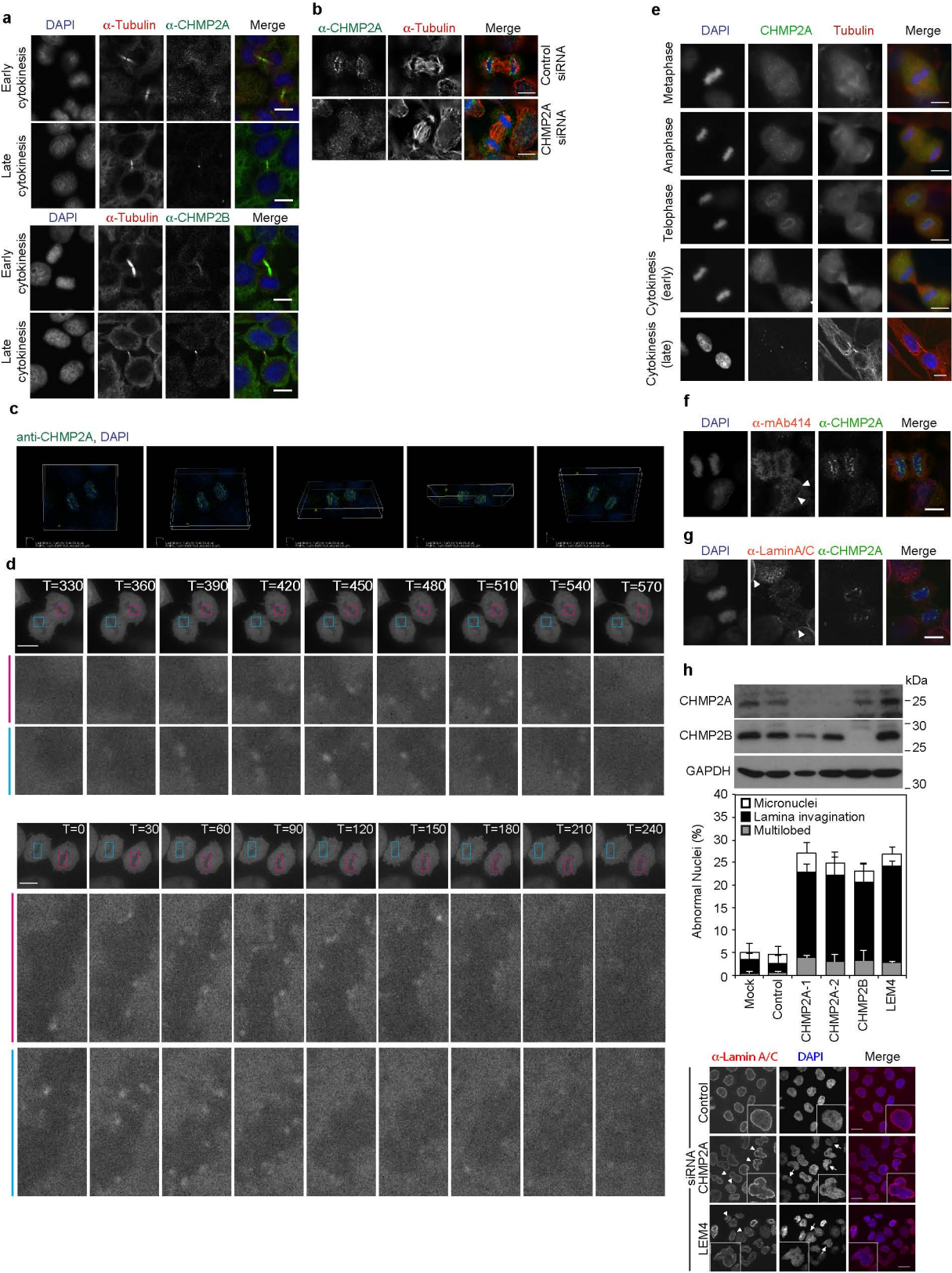

Olmos et al., ED Figure 2

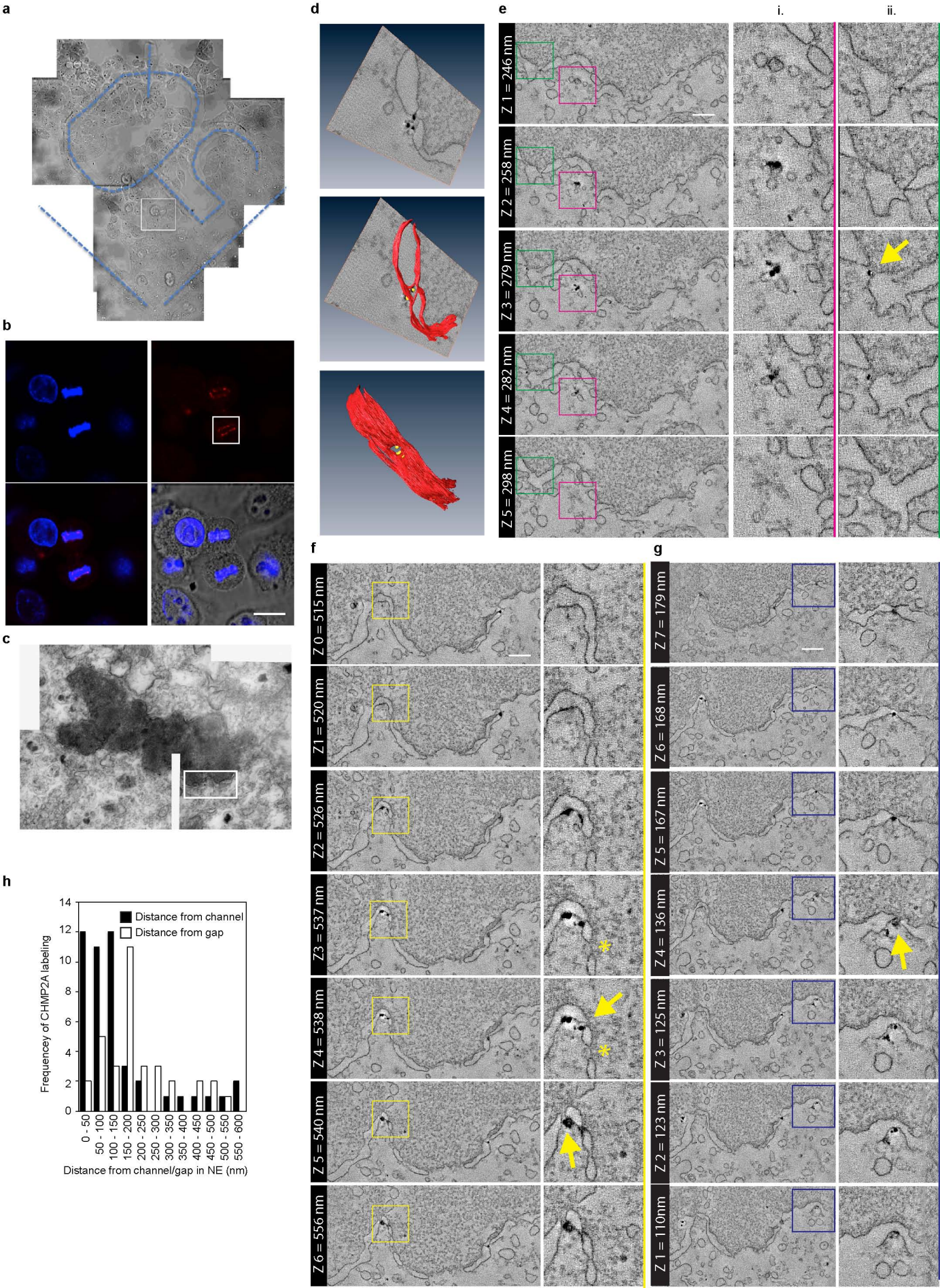

Olmos et al., ED Figure 3

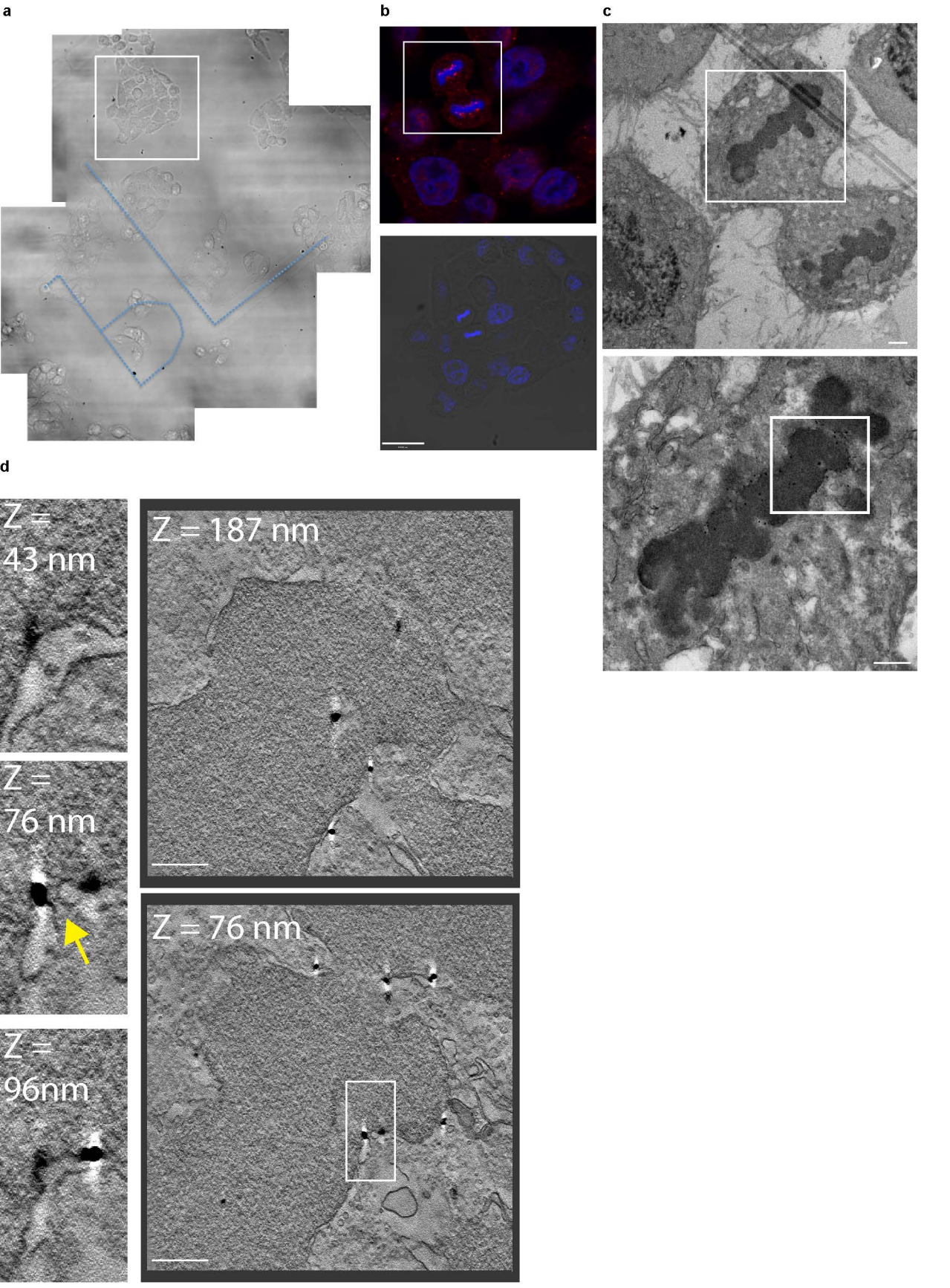

Olmos et al., ED Figure 4

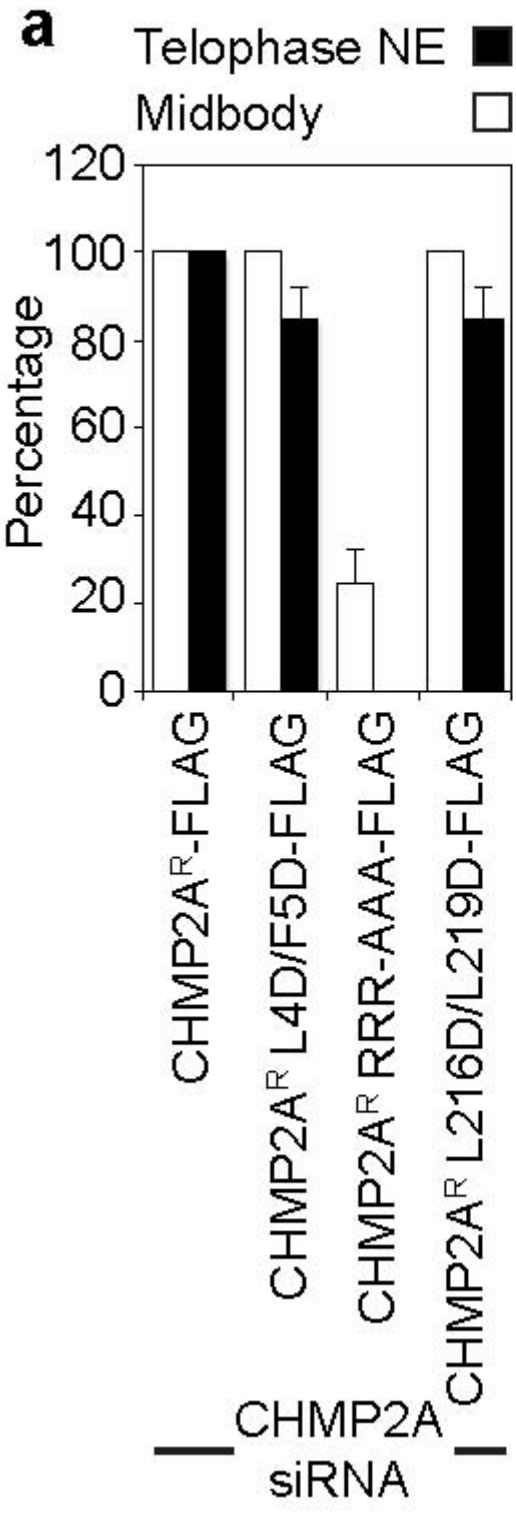

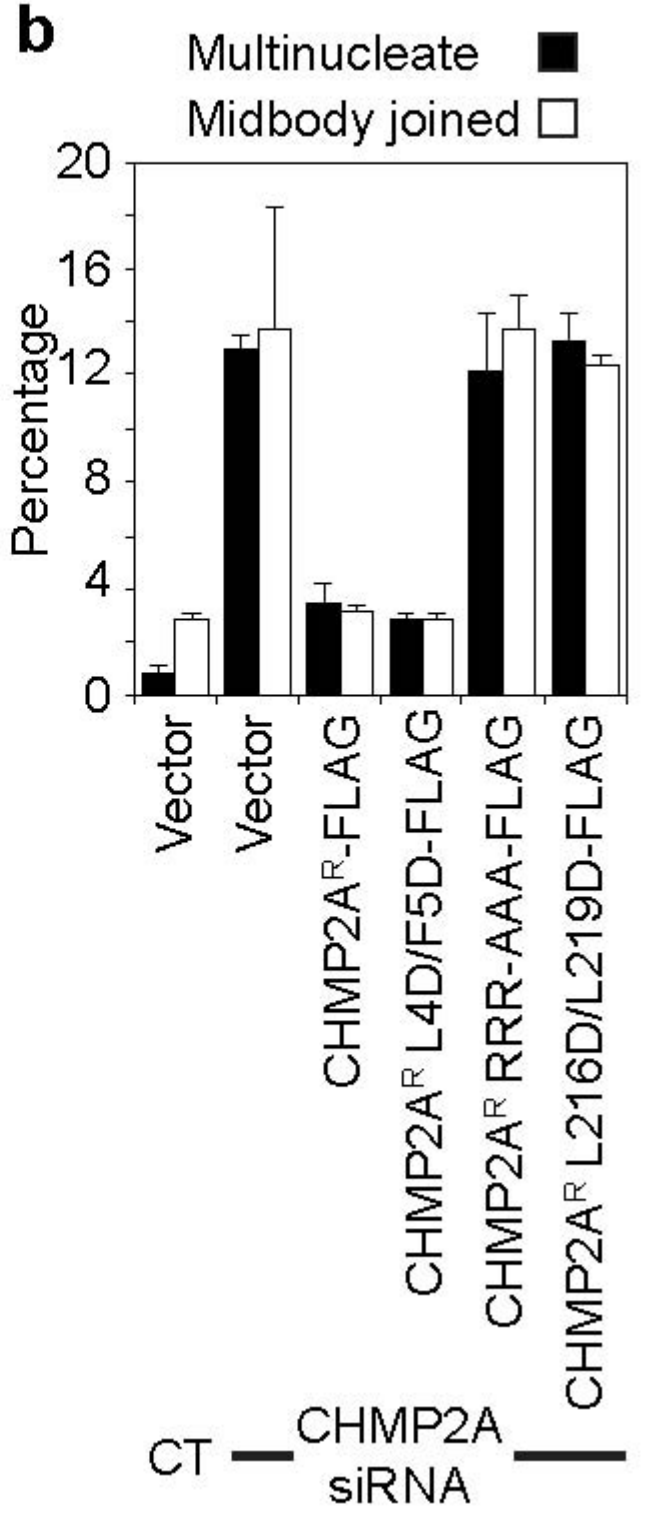

Olmos et al., ED Figure 5

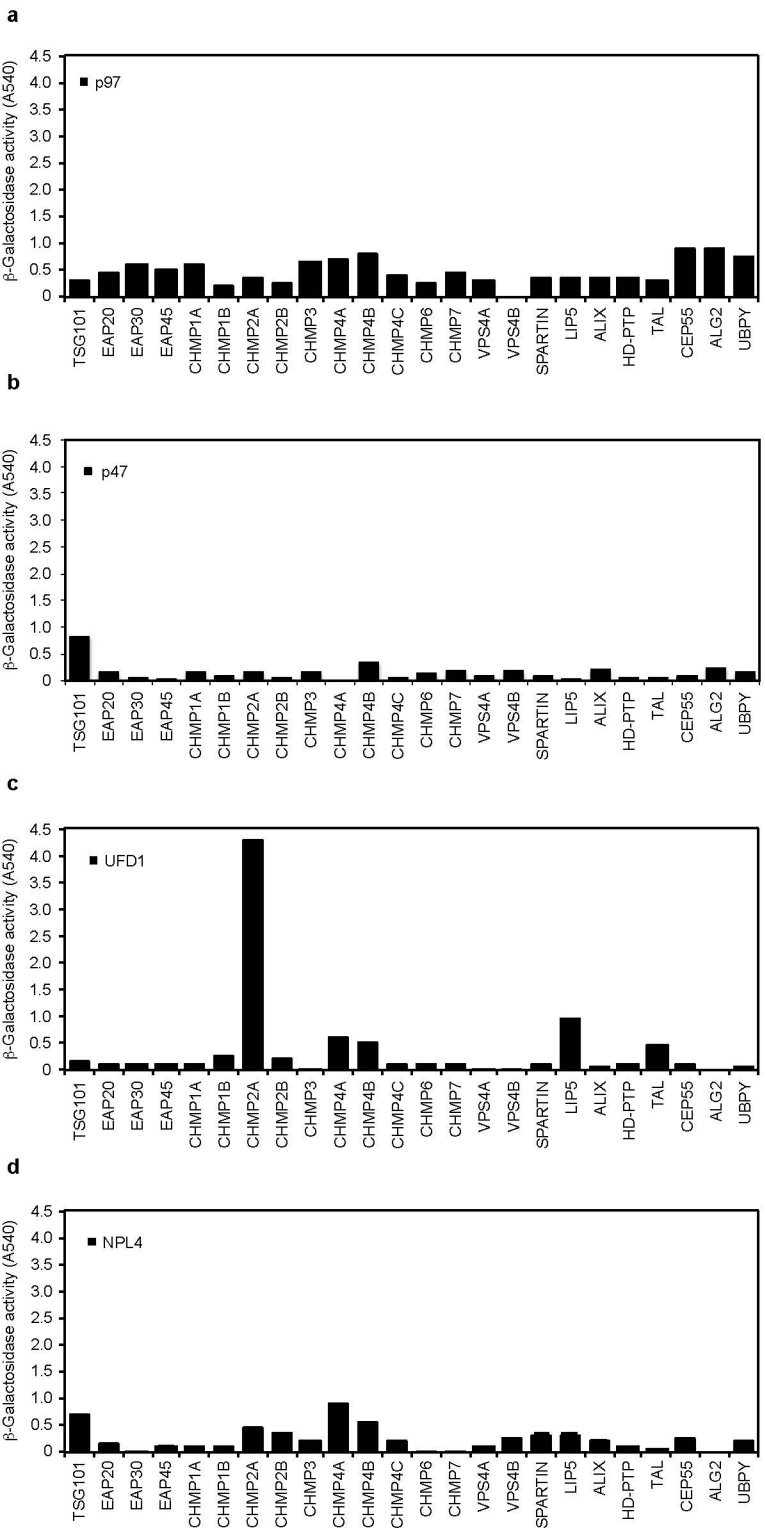

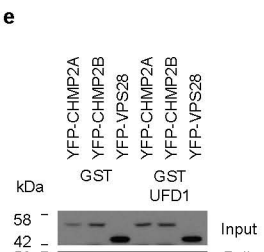

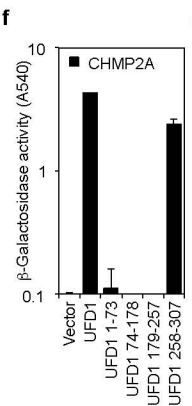

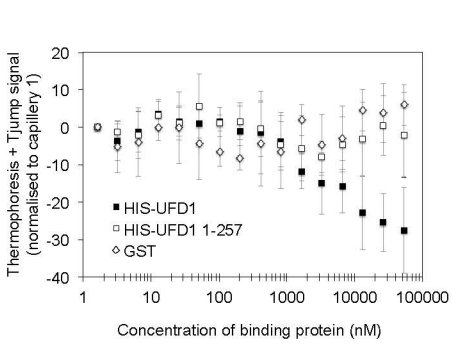

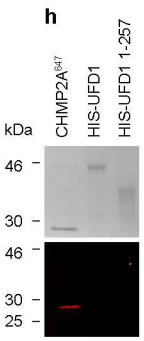

Olmos et al., ED Figure 6

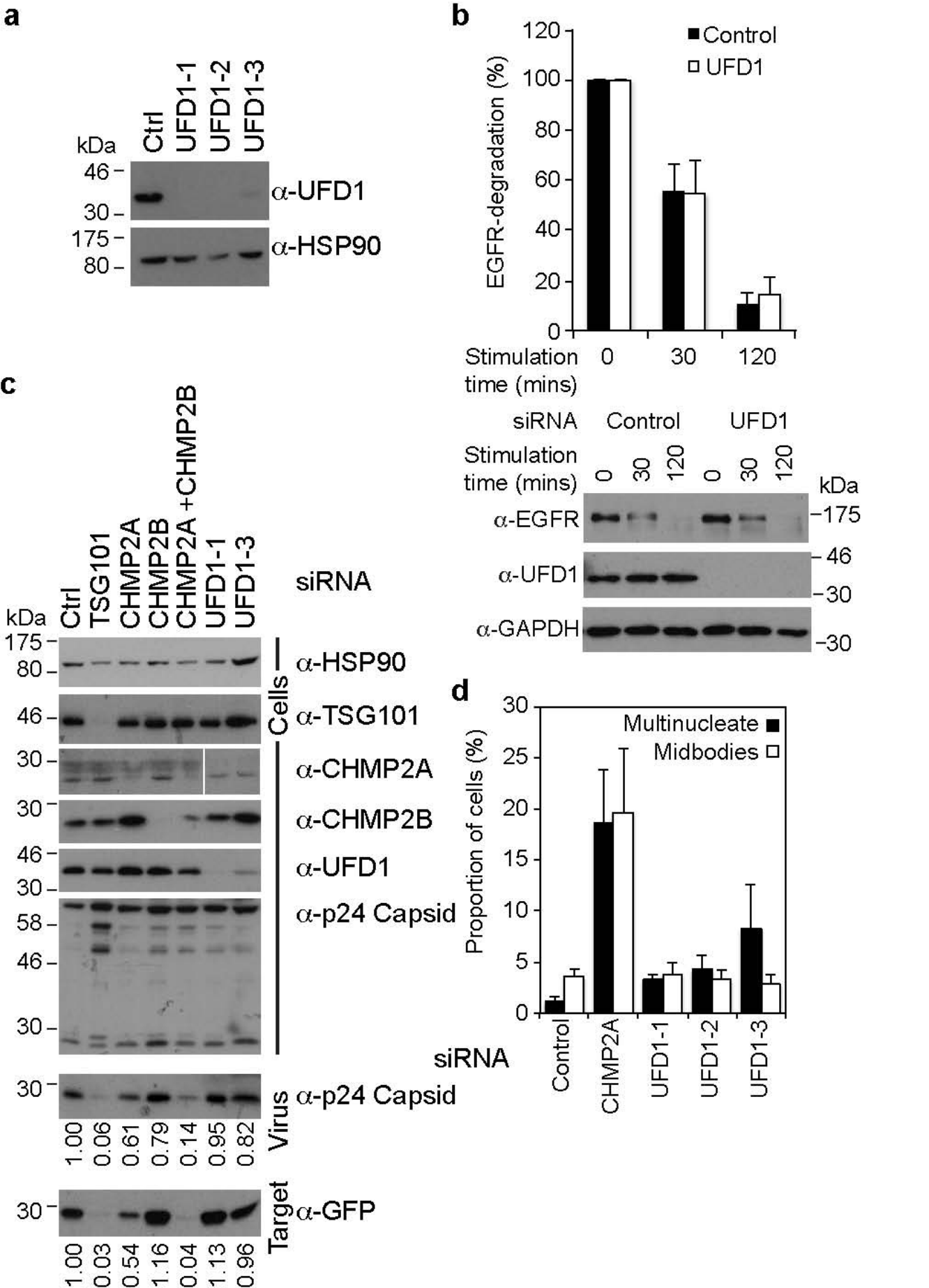

Olmos et al., ED Figure 7

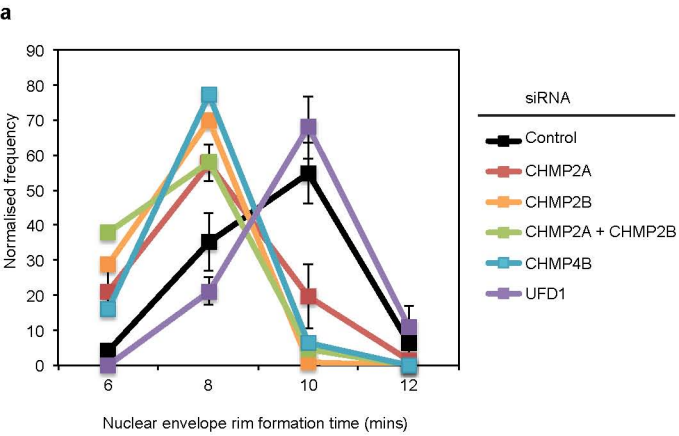

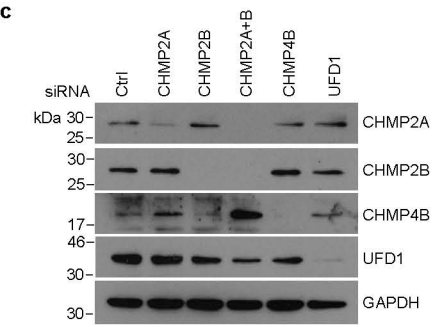

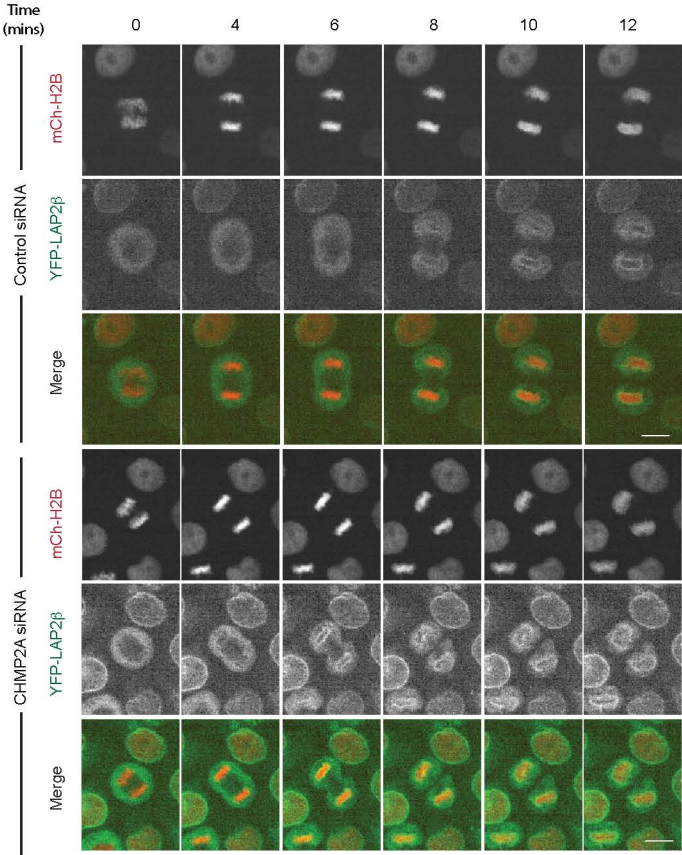

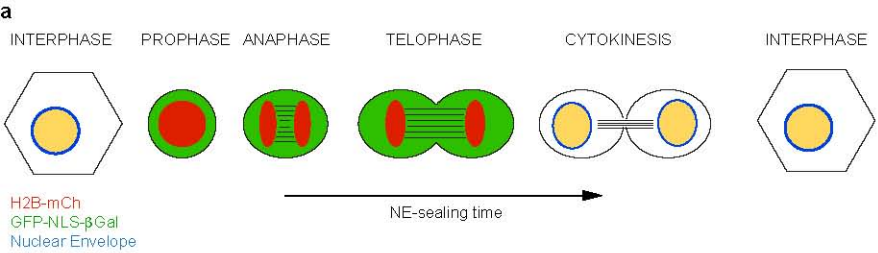
a
INTERPHASE
PROPHASE
ANAPHASE
TELOPHASE
CYTOKINESIS
INTERPHASE
H2B-mCh
GFP-NLS-βGal
Nuclear Envelope
NE-sealing time

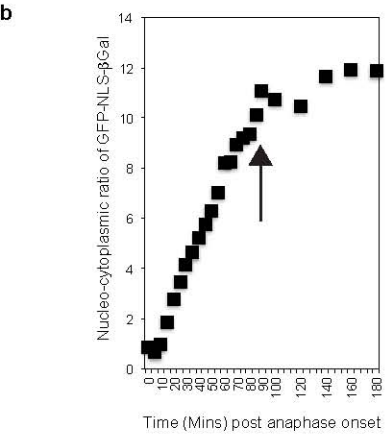
b
Nucleo-cytoplasmic ratio of GFP-NLS-βGal
Time (Mins) post anaphase onset

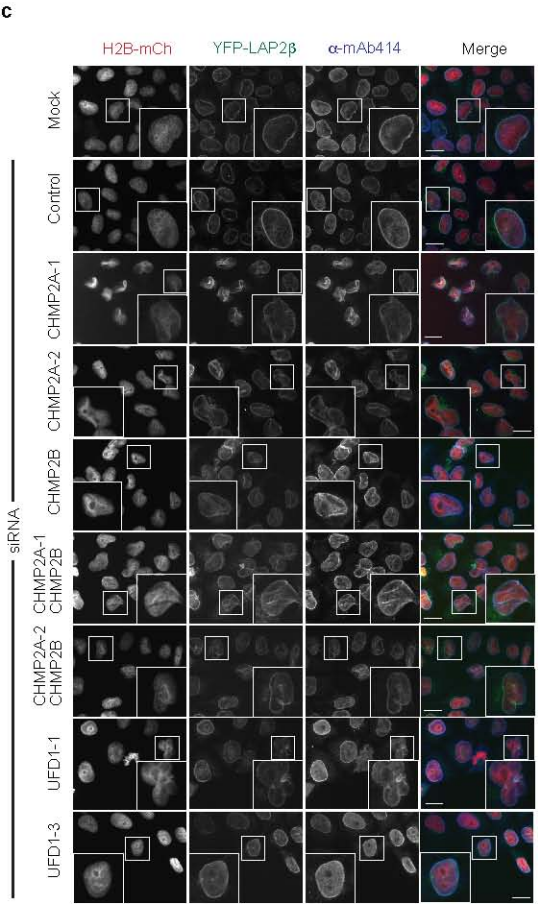
c
H2B-mCh
YFP-LAP2β
α-mAb414
Merge
Mock
Control
CHMP2A-1
CHMP2A-2
CHMP2B
CHMP2A-1 CHMP2B
CHMP2A-2 CHMP2B
UFD1-1
UFD1-3
siRNA

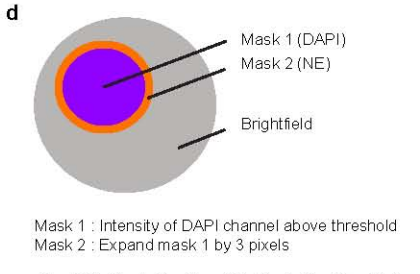
d
Mask 1 (DAPI)
Mask 2 (NE)
Brightfield
Mask 1 : Intensity of DAPI channel above threshold
Mask 2 : Expand mask 1 by 3 pixels
Alexa594 (Mask 2) - Alexa594 (Mask 1) = NE staining

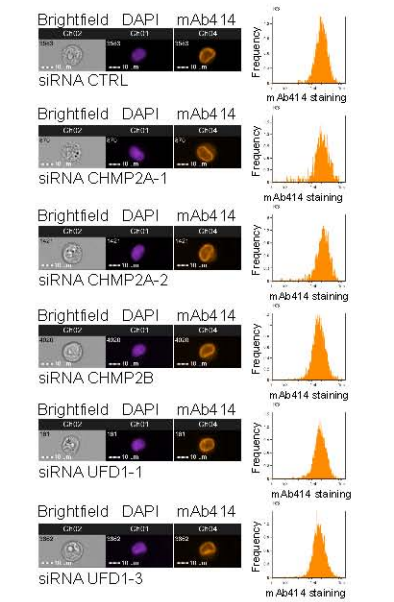
e
Brightfield
DAPI
mAb414
siRNA CTRL
siRNA CHMP2A-1
siRNA CHMP2A-2
siRNA CHMP2B
siRNA UFD1-1
siRNA UFD1-3
Frequency
mAb414 staining

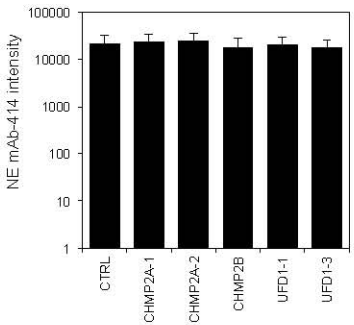
NE mAb-414 intensity
CTRL
CHMP2A-1
CHMP2A-2
CHMP2B
UFD1-1
UFD1-3

Olmos et al., ED Figure 9

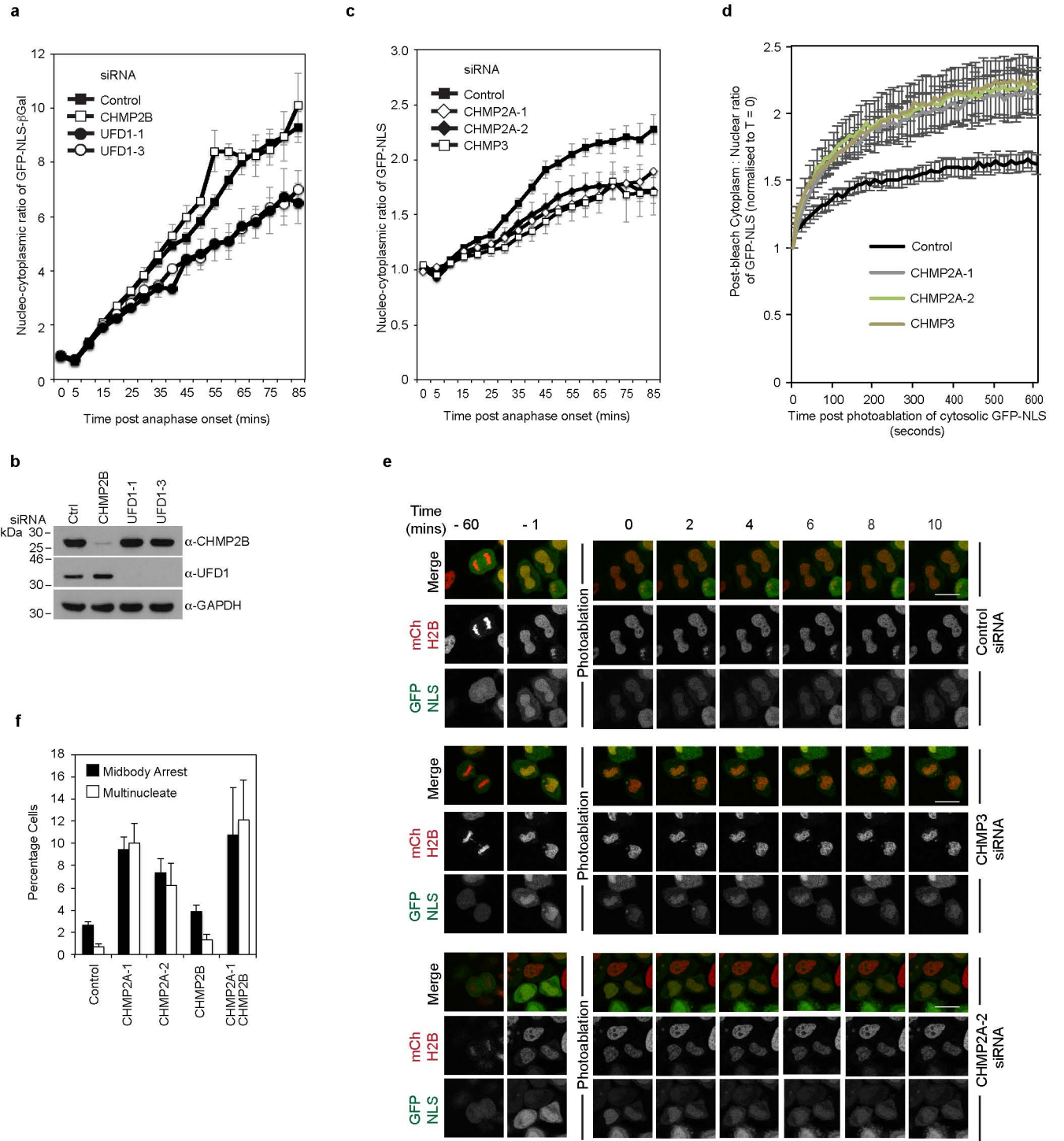

Olmos et al., ED Figure 10

a

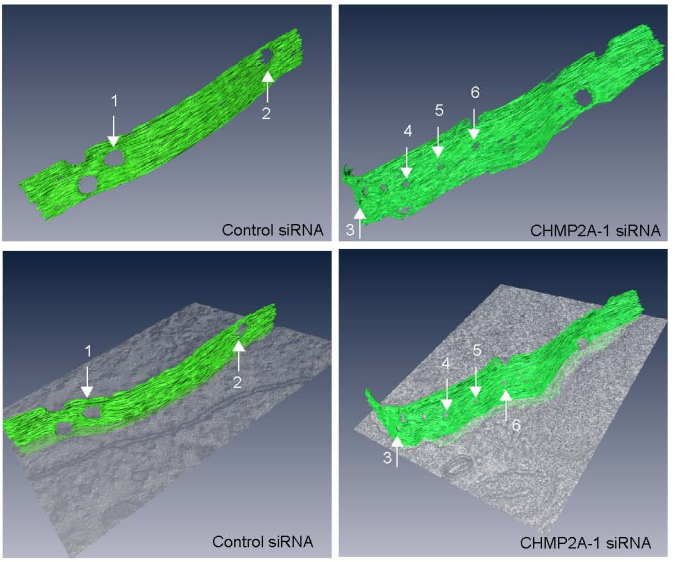

b

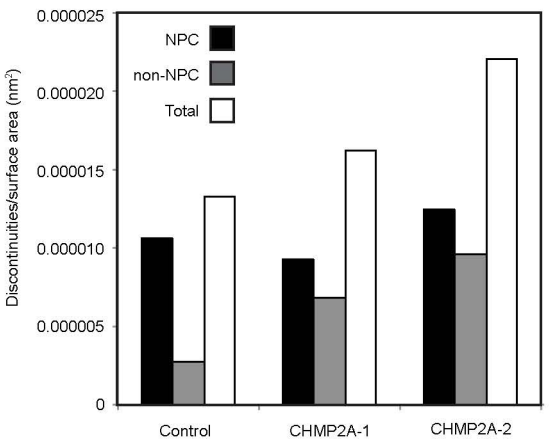

c